AGU PUBLICATIONS

Global Biogeochemical Cycles

RESEARCH ARTICLE

10.1002/2017GB005714

Key Points:

- Observed CO_2 and H_2O fluxes from forest sites in China were used to optimize model parameters of a global terrestrial ecosystem model
- Optimized parameters alter the simulated sensitivity of forest carbon dynamics to warming and altered precipitation
- Independent evaluation suggests that modification in model structure is needed for improving prediction of long-term forest carbon dynamics

Supporting Information:

- Supporting Information S1

Correspondence to:
S. Piao,
slpiao@pku.edu.cn

Citation:
Li, Y., H. Yang, T. Wang, N. MacBean, C. Bacour, P. Ciais, Y. Zhang, G. Zhou, and S. Piao (2017), Reducing the uncertainty of parameters controlling seasonal carbon and water fluxes in Chinese forests and its implication for simulated climate sensitivities, *Global Biogeochem. Cycles*, *31*, 1344–1366, doi:10.1002/2017GB005714.

Received 10 MAY 2017
Accepted 14 AUG 2017
Accepted article online 16 AUG 2017
Published online 31 AUG 2017

Reducing the uncertainty of parameters controlling seasonal carbon and water fluxes in Chinese forests and its implication for simulated climate sensitivities

Yue Li[1], Hui Yang[1], Tao Wang[2,3], Natasha MacBean[4], Cédric Bacour[5,6], Philippe Ciais[5], Yiping Zhang[7], Guangsheng Zhou[8,9], and Shilong Piao[1,2,3]

[1]Sino-French Institute for Earth System Science, College of Urban and Environmental Sciences, Peking University, Beijing, China, [2]Key Laboratory of Alpine Ecology and Biodiversity, Institute of Tibetan Plateau Research, Chinese Academy of Sciences, Beijing, China, [3]CAS Center for Excellence in Tibetan Plateau Earth Sciences, Chinese Academy of Sciences, Beijing, China, [4]School of Natural Resources and the Environment, University of Arizona, Tucson, Arizona, USA, [5]Laboratoire des Sciences du Climat et de l'Environnement, CEA CNRS, UVSQ, Gif-sur-Yvette, France, [6]NOVELTIS, Labège, France, [7]Key Laboratory of Tropical Forest Ecology, Xishuangbanna Tropical Botanical Garden, Chinese Academy of Sciences, Mengla, China, [8]Chinese Academy of Meteorological Sciences, Beijing, China, [9]State Key Laboratory of Vegetation and Environmental Change, Institute of Botany, Chinese Academy of Sciences, Beijing, China

Abstract Reducing parameter uncertainty of process-based terrestrial ecosystem models (TEMs) is one of the primary targets for accurately estimating carbon budgets and predicting ecosystem responses to climate change. However, parameters in TEMs are rarely constrained by observations from Chinese forest ecosystems, which are important carbon sink over the northern hemispheric land. In this study, eddy covariance data from six forest sites in China are used to optimize parameters of the ORganizing Carbon and Hydrology In Dynamics EcosystEms TEM. The model-data assimilation through parameter optimization largely reduces the prior model errors and improves the simulated seasonal cycle and summer diurnal cycle of net ecosystem exchange, latent heat fluxes, and gross primary production and ecosystem respiration. Climate change experiments based on the optimized model are deployed to indicate that forest net primary production (NPP) is suppressed in response to warming in the southern China but stimulated in the northeastern China. Altered precipitation has an asymmetric impact on forest NPP at sites in water-limited regions, with the optimization-induced reduction in response of NPP to precipitation decline being as large as 61% at a deciduous broadleaf forest site. We find that seasonal optimization alters forest carbon cycle responses to environmental change, with the parameter optimization consistently reducing the simulated positive response of heterotrophic respiration to warming. Evaluations from independent observations suggest that improving model structure still matters most for long-term carbon stock and its changes, in particular, nutrient- and age-related changes of photosynthetic rates, carbon allocation, and tree mortality.

1. Introduction

Process-based terrestrial ecosystem models (TEMs) are used for estimating global/regional carbon budgets [*Pacala et al.*, 2001; *Morales et al.*, 2007; *Le Quéré et al.*, 2009; *Piao et al.*, 2009], for attributing ecosystem responses to increasing atmospheric CO_2 and climate change [*Cramer et al.*, 2001; *McGuire et al.*, 2001; *Piao et al.*, 2015; *Huang et al.*, 2015; *Zhu et al.*, 2016] and for projecting future climate-carbon cycle feedback via coupling with general circulation models [*Friedlingstein et al.*, 2006; *Sitch et al.*, 2008; *Arora et al.*, 2013]. The results from land surface models are affected by uncertainties from model structure [*Shugart et al.*, 2010; *Antonarakis et al.*, 2014], initial condition definitions [*Carvalhais et al.*, 2010], climate forcing [*Berthelot et al.*, 2005; *Zhao et al.*, 2012], spatial resolution [*Potter et al.*, 2013; *Pappas et al.*, 2015], and parameter values [*LeBauer et al.*, 2013]. In parallel with the incorporation of new processes, parameter uncertainty needs to be reduced as it explains a large proportion of the variance of vegetation carbon fluxes and storage through photosynthesis, respiration, carbon turnover rates, and water balance [*Knorr and Heimann*, 2001; *Zaehle et al.*, 2005; *Pappas et al.*, 2013]. Meanwhile, the tendency to incorporate new processes introduces more uncertain parameters, possibly further increasing the spread of model results during the development stage [*Prentice et al.*, 2015]. Therefore, assimilating observed information to optimize model parameters is necessary and should be frequently repeated when the new parameters are introduced during the model development.

Eddy flux towers measure ecosystem-scale CO_2, energy, and water fluxes, which can be used for constraining model parameters and consequently improving TEMs performance [*Baldocchi et al.*, 2001; *Williams et al.*, 2009]. A pioneer work by *Wang et al.* [2001] found that a key parameter common to the photosynthesis scheme of most land surface models, J_{max} (electron transport capacity), was best determined by incorporating the diurnal variation of 3 week mean net CO_2 flux measured at six paired crop-pasture sites in southeast Australia. Applying a similar gradient-based parameter optimization method, *Reichstein et al.* [2003] estimated photosynthetic parameters at three Mediterranean sites and emphasized that the estimation of leaf-level parameters should not ignore the observed H_2O (i.e., latent heat) flux, either. More recently, the application of Bayesian optimization allowed a variety of uncertain parameters to be considered in one cost function using both the observed CO_2 and H_2O fluxes of forests involved with different plant functional types (PFTs) in North America [*Braswell et al.*, 2005; *Knorr and Kattge*, 2005], Europe [*Friend et al.*, 2007; *Santaren et al.*, 2007, 2014; *Bacour et al.*, 2015], and in the Amazon [*Verbeeck et al.*, 2011]. Despite differences in the number and type of constrained parameters in each study, the advantage of eddy covariance measurements has been demonstrated in terms of improving site-level simulations of CO_2 and H_2O fluxes in both simple and complex models [*Jarvis et al.*, 2004; *Williams et al.*, 2005; *Wang et al.*, 2007].

However, to our knowledge, only a few studies have paid attention to assimilating the seasonal cycle of observed fluxes from Chinese forest ecosystems, which have been shown as an important carbon sink over the northern hemispheric land [e.g., *Piao et al.*, 2005], in particular, subtropical forests [*Yu et al.*, 2014]. Typical applications of a better seasonal model include improved simulations of river discharge and water budgets in China and better prior estimates of the net carbon exchange for atmospheric CO_2 inversion studies [e.g., *Peylin et al.*, 2013]. Due to lack of the observational constraints, currently simulated carbon and water fluxes from these ecosystems are thus uncertain [*Piao et al.*, 2012]. Although several parameter optimization studies are based on multisite/multi-PFT assimilations of observed CO_2 and H_2O fluxes from the FLUXNET global network [*Kuppel et al.*, 2014; *Peylin et al.*, 2016; *Raoult et al.*, 2016], the corresponding optimized parameters may not be representative for China because FLUXNET only contains very few Chinese forest sites and the estimated parameters have been shown to vary from site to site [*Groenendijk et al.*, 2011; *Xiao et al.*, 2011]. To our knowledge, one model parameter optimization only has, so far, been performed in China, for a coniferous forest [*Ju et al.*, 2010]. Considering the special Asian monsoon climate which brings plenty of water and heat resources during the growing season [*Yu et al.*, 2014], whether the CO_2 and H_2O fluxes from a variety of forest types in China can be captured by the optimized TEM or not still remains an unknown issue.

The impact of climate change on Chinese forest ecosystem has not been fully quantified due to lack of measurements (e.g., manipulation experiments) [*Wu et al.*, 2011, Figure 1; *Lu et al.*, 2013a], and it is therefore unknown whether the responses of forest carbon cycles to changed climate are adequately represented in the current TEMs. Uncertainty thus still persists within the current state-of-the-art carbon cycle models [e.g., *Peng et al.*, 2009], although they have been shown to be able to qualitatively reproduce the terrestrial ecosystem response to changed environmental factors compared to some manipulative experiments [*Luo et al.*, 2008]. Accurate quantification of sensitivity of the simulated terrestrial carbon cycle processes to altered climate, however, remains a bottleneck ([e.g., *T. Wang et al.*, 2011; *X. Wang et al.*, 2014; *Wang et al.*, 2017] models inability to reproduce the observed response of carbon cycle to climate variability on interannual scales and on regional spatial pattern) for accurately estimating regional climate-carbon cycle feedback, which will in part influence the climate in the future [*Luo*, 2007; *Piao et al.*, 2013]. Although the assumption-centered approach [see *Medlyn et al.*, 2015] can be used to utilize data from ecosystem experiments to reduce the model uncertainty, however, improvements of regional model applied in China would need local experiment data, which are currently rare. Consequently, the optimized TEM not only provides us the potential of looking into the impact of climate change on forests in China but also enables us to further quantify the uncertainty brought by parameters in terms of the modeled response to altered temperature and precipitation, which is rarely considered in previous studies [e.g., *Gerten et al.*, 2008].

In this study, we optimized parameters of the ORCHIDEE (ORganizing Carbon and Hydrology In Dynamics EcosystEms) TEM [*Krinner et al.*, 2005; *Peylin et al.*, 2016] related to photosynthesis, respiration, and phenology processes using eddy covariance data from six forest sites (five PFTs) in China. The optimized model is further applied to investigate the change of the model response to hypothetical changes in temperature and precipitation amount. We aim to address the following scientific questions: (1) How well does the optimized model

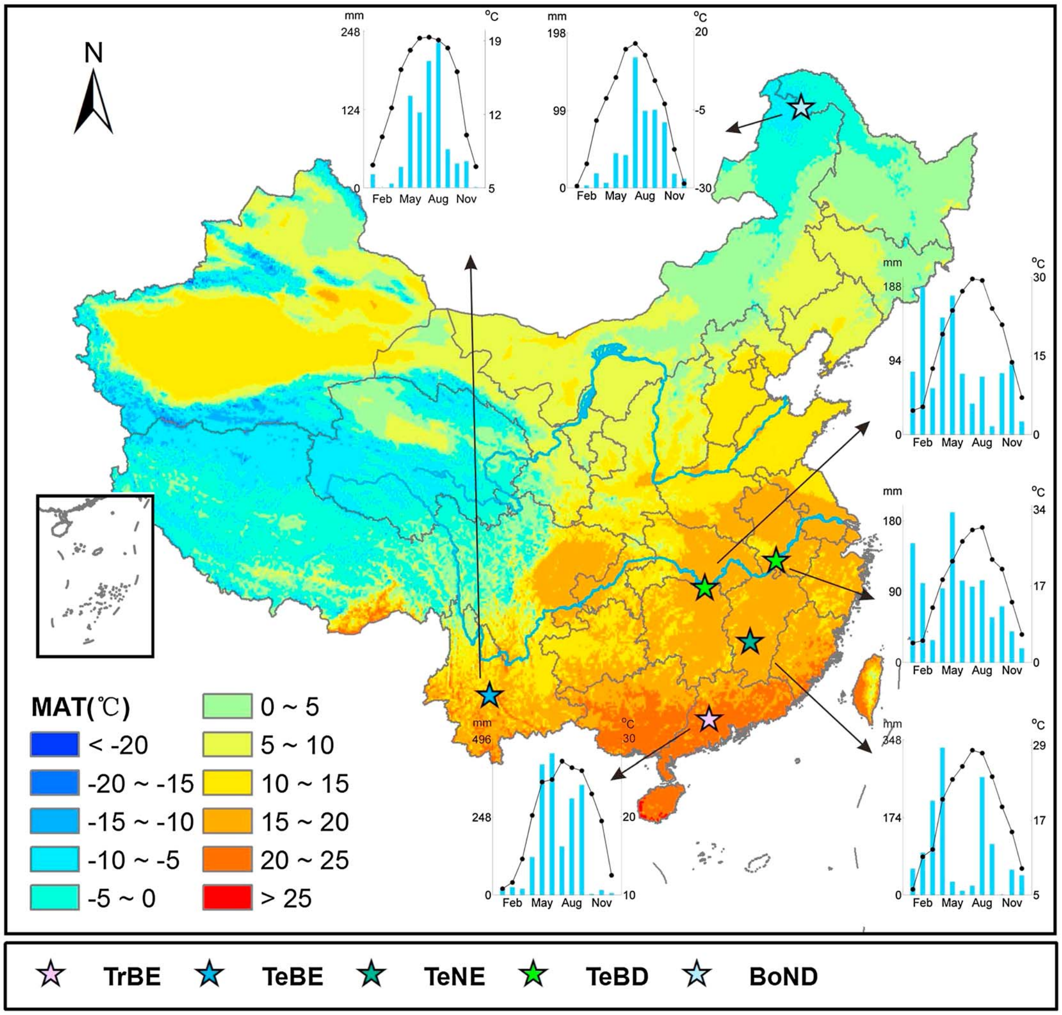

Figure 1. Locations of the six eddy covariance flux sites dominated by five forest types in China. The plant functional type (PFT) for each site is defined based on their climate zones, vegetation phenology type, and physiognomy (see Table S1). The seasonal cycle of the monthly temperature and precipitation are also shown beside the map of the climatological mean annual temperature (MAT, derived from the China forcing data set over 1981–2010) for each site and for the year when the model's parameters are optimized.

describe the temporal dynamics (in particular, the seasonal cycle) of CO_2 and H_2O fluxes measured from forest ecosystems in China? (2) What is the impact of flux assimilation on the model parameters? (3) To what extent does the optimized parameter set affect the model response of ecosystem carbon fluxes to altered temperature and precipitation?

2. Materials and Methods

2.1. Forest Sites in China

Six forest sites were selected to provide the observed fluxes and meteorological forcing in this study (Table S1 in the supporting information and Figure 1). Based on their climate zones, vegetation phenology type, and physiognomy, the vegetation types of these sites are classified into five categories: tropical evergreen broadleaf forest (TrBE, in Dinghushan (DHS)) [*Yu et al.*, 2006], temperate evergreen broadleaf forest (TeBE, in Ailaoshan (AIL)) [*Zhang et al.*, 2010], temperate evergreen needleleaf forest (TeNE, in Qianyanzhou (QYZ)) [*Yu et al.*, 2006], temperate deciduous broadleaf forest (TeBD, in Hunan Yueyang (HNY) and Anhui Huaining (ANH)) [*Zhou et al.*, 2011] and boreal deciduous needleleaf forest (BoND in Huzhong (HUZ)) [*Wang et al.*, 2010]. These sites generally represent the main forest types in China and span a relatively wide range of climate zones in China: Mean annual temperatures (MAT) decrease from 22.5°C to −2.2°C along with increased latitude and mean annual precipitations (MAP) are higher for sites in southern China (>800 mm) than in northeastern China (<800 mm) (Table S1). Temperatures and precipitations at the six sites have similar seasonal cycle, with abundant precipitation usually occurring over spring and summer periods due to the activity of the East Asia monsoon system (Figure 1). More detailed information on the forest sites including site history and canopy height can be found in descriptions from references that are listed in Table S1.

2.2. Data and Processing

2.2.1. Carbon and Water Fluxes

Measured half-hourly net ecosystem exchange (NEE) and latent heat (LE) for 3 years at TrBE site in DHS and for 2 years at the other sites (Table S1) are used in this study. Detailed gap-filling methods and quality flag were only provided for two sites (TeBD HNY and ANH) from the global FLUXNET data set (http://www.fluxdata.org/), and a large proportion of gaps remains in the data from other sites accessed from the ChinaFLUX (http://www.chinaflux.org/enn/index.aspx) or the AsiaFLUX (http://www.asiaflux.net/) sites. To obtain a relatively continuous record, measured NEE and LE time series at these sites were firstly gap filled, and NEE was then partitioned into gross primary production (GPP) and ecosystem respiration (R_{eco}) through algorithms described in *Reichstein et al*. [2005] using the eddy covariance gap-filling and flux-partitioning software available online (http://www.bgc-jena.mpg.de/~MDIwork/eddyproc/index.php). Because the method of friction velocity (u^*) correction is controversial [*Papale et al*., 2006; *Baldocchi*, 2008] and not all the sites provide the variable u^*, we disabled this option during the gap-filling processing. Although GPP is termed an observation in this study, one should keep in mind that this flux is, in fact, deduced from NEE with an empirical model and therefore not directly measured at any of the forest sites.

2.2.2. Meteorological Forcing

Driving the ORCHIDEE model needs quasi-continuous meteorological forcing (see Table S2) with a temporal resolution of 30 min. If the temporal interval of the forcing data is longer than that, the model interpolates the meteorological fields into half-hourly fields. Some original meteorological observations were missing for each site, and data gaps exist in these records. We thus reconstructed the site-level meteorological forcing by complementing observed records with data from the China meteorological forcing data set (3 h interval, 0.1° × 0.1° grid over China, 1979–2015) [*He*, 2010]. This China forcing data set was produced by merging observed meteorological records (particularly, observed wind, air temperature, relative humidity, sunshine duration, precipitation, and surface pressure over stations in China) with the model reanalysis from Princeton forcing data [*Sheffield et al*., 2006]. *Chen et al*. [2011] showed that this data set has reduced biases in the simulated land surface temperature in China compared to the Global Land Data Assimilation System forcing data. The reconstruction of 3 h site-level meteorological forcing is performed in the following steps:

First, the half-hour meteorological variables from site observed records are resampled (for temperature, specific humidity, surface pressure, and wind speed), averaged (for downward shortwave radiation and longwave radiation), or accumulated (for precipitation) every 3 h to match the temporal resolution from the China forcing data set. Then, the China forcing data set is corrected using available site data with a linear regression equation, given that there is a scale mismatch between site measurements and the China forcing data set over the corresponding pixels. Then, the linear regression equation is applied to correct the China forcing data set and the corrected series is used to fill the gaps in the observed records. For precipitation, we fill the gaps with data directly extracted from the China forcing data set and constrain the annual precipitation amount to match the annual precipitation from either the site or the nearest meteorological station (data available from 1981 to 2010). Note that the reconstruction is applicable to the TrBE, TeNE, and two TeBD sites. For the two other forest types (i.e., TeBE and BoND) where all the meteorological variables are missing, the forcing of the sites is directly replaced by corresponding pixel values from the China forcing data set.

2.3. The ORCHIDEE Data Assimilation System

The model-data fusion framework used in this study is called the ORCHIDEE Data Assimilation System (ORCHIDAS, https://orchidas.lsce.ipsl.fr/index.php), which consists of the ORCHIDEE TEM and a Bayesian inversion framework [e.g., *Kuppel et al*., 2014; *Bacour et al*., 2015; *MacBean et al*., 2015; *Peylin et al*., 2016]. The ORCHIDEE model includes processes of the terrestrial carbon cycle, vegetation dynamics, and the energy, water, and momentum exchange between the atmosphere and biosphere [*Krinner et al.*, 2005]. This model can be either forced in an "off-line" mode by climate forcing data or coupled to an atmospheric model to simulate the fluxes from the land surface globally and regionally. The latest trunk version (Revision 3035) of ORCHIDEE is used here to simulate site-level CO_2 (NEE and GPP) and LE fluxes in this study. To perform a simulation at each forest site, we prescribe the vegetation fraction and set the soil texture parameters according to the high spatial resolution soil database of *Shangguan et al.* [2014] based on the 1 million scale Soil Map of China. Then, we drive the model forced by the reconstructed 3-hourly (the forcing is interpolated to 30 min within the model) gap-filled meteorological measurements at each site. The meteorological forcing and CO_2 concentration during the data period of each site is repeatedly cycled until the vegetation biomass and soil carbon pool reach equilibrium [see also *Santaren et al.*, 2014; *Kuppel et al.*, 2014].

The optimization follows a Bayesian inversion framework. An optimal parameter set is obtained finding the minimum of a cost function defined by the sum of the mismatch between (1) simulated and observed fluxes and (2) the prior and optimized parameters [*Peylin et al.*, 2016, equation (1)] weighted by their respective errors. The observation error covariance matrix that accounts both for measurement uncertainties and model structural errors, is determined as the root-mean-square error (RMSE) between the prior simulations and the observations as in *Kuppel et al*. [2014]; and the prior uncertainty on model parameters is defined as 40% of the prior parameter range for parameter term as in *Bacour et al*. [2015]. The cost function is minimized through a gradient-based algorithm called L-BFGS [*Byrd et al*., 1995], with its setting following *Kuppel et al*. [2012, 2014]. In this study, we include the GPP together with measured NEE and LE in the cost function due to the interest of improving the model's capability to reasonably simulate the vegetation productivity as well as the carbon and water fluxes. At each site, daily NEE, LE, and partitioned GPP for the year of optimization (i.e., the optimization year, Table S1) are flagged as the good quality data if the daily value is computed from the half-hourly data with less than 50% gaps within a day (see section 2.4.2). The same quality filtering was applied to data from the other years that are not used to optimize the parameters but reserved for cross-year validation. Following previous studies [*Kuppel et al*., 2014; *Bacour et al*., 2015], we define the observation errors as the RMSE of fluxes between observations and the prior simulations during the optimization year.

2.4. Analysis

2.4.1. Sensitivity Analysis and Parameter Selection

The ORCHIDEEv3035 version has updated many key processes as well as new parameters related to photosynthesis, autotrophic respiration (R_a), heterotrophic respiration (R_h), phenology, and soil water availability. Previous ORCHIDEE optimization studies used a parameter set consistent with a previous version (e.g., the "AR5" version used, for instance, in *Kuppel et al*. [2014] and *Peylin et al*. [2016]). Therefore, in this study we first perform a sensitivity analysis using the Morris method [e.g., *Lu et al*., 2013b] to select the most important parameters for ORCHIDEEv3035 through ranking parameters by their mean effect (i.e., change in NEE, LE, and GPP resulted from relative change in parameters) on the model output (i.e., NEE, LE, and GPP in this study, see detailed steps of this method in *Lu et al*. [2013b]). For each site, the 10 most influential PFT-specific parameters for NEE, LE, and GPP are separately selected, to generate the parameter set for each PFT (Table S3 for the parameter description and Table S4 for the prior ranges for each PFT). These selected parameters are then optimized at each site using the ORCHIDAS optimization scheme. The prior parameter range (see Table S4) is determined based on minimum prior standard deviation (usually 40% of the prior value) and literature analysis (http://forge.ipsl.jussieu.fr/orchidee/wiki/Documentation/UserGuide, parameters range table).

2.4.2. Evaluation Metrics and Independent Observations

Following previous studies [*Kaminski et al*., 1996; *Peng et al*., 2015], we define the following metrics at daily or monthly time scales to assess the difference between observations and simulations (including prior and posterior (i.e., optimized) simulations, corresponding to parameters before and after optimization, respectively), as well as the simulated seasonal cycle of the fluxes:

Root-mean-square error (RMSE):

$$\mathrm{RMSE} = \sqrt{\frac{1}{n}\sum_{i=1}^{n}\left(\alpha_i^{\mathrm{sim}} - \alpha_i^{\mathrm{obs}}\right)^2} \quad (1)$$

Mean bias (MB):

$$\mathrm{MB} = \frac{1}{n}\sum_{i=1}^{n}\left(\alpha_i^{\mathrm{sim}} - \alpha_i^{\mathrm{obs}}\right) \tag{2}$$

Amplitude bias (AB):

$$\mathrm{AB} = \alpha_{\mathrm{amplitude}}^{\mathrm{sim}} - \alpha_{\mathrm{amplitude}}^{\mathrm{obs}} \tag{3}$$

Agreement of the seasonal cycle (F_s):

$$F_s = \frac{\left\langle \boldsymbol{\alpha}^{sim}, \boldsymbol{\alpha}^{\mathrm{obs}} \right\rangle}{\left\langle \boldsymbol{\alpha}^{\mathrm{obs}}, \boldsymbol{\alpha}^{\mathrm{obs}} \right\rangle}, \tag{4}$$

where α_i^{sim} and α_i^{obs} are the simulated and observed fluxes at the ith day of 1 year, respectively; $\alpha_{amplitude}^{sim}$ and $\alpha_{amplitude}^{obs}$ denote the seasonal amplitude (defined as the difference between the maximum and minimum monthly mean values) of simulated and observed fluxes, respectively; and $\boldsymbol{\alpha}^{sim}$ and $\boldsymbol{\alpha}^{obs}$ are 12-tuple vectors containing the monthly anomaly values (i.e., monthly mean subtracted by annual mean) of simulated and observed fluxes (excluding NEE), respectively. The symbol $<,>$ denotes the inner product of two vectors. For a better model-data fit, the MB, RMSE, and AB are expected to be close to 0, and F_s should approach 1, beyond which the simulations are expected to overestimate the observation and vice versa.

To quantify the improvement of the seasonal cycle agreement index as a result of the optimization, we further subtract the absolute value of the difference between 1 and F_s for the prior simulations by the same metric obtained with the optimized simulations to obtain an improvement-indicated index so called I_i (i.e., positive value denotes an improvement and vice versa). To exclude the potential impact of low-quality data on the model evaluation, any daily value having more than 50% gaps of half-hourly values within a day is flagged as the low quality and excluded from the observed record (and also from the corresponding simulation) when calculating all metrics. But this criterion cannot be applied over the AIL site where the observed daily data are only available without any quality control.

We also use three independent observation data, namely, the soil organic carbon (SOC) density in top 1 m, the aboveground tree biomass, and the satellite-derived leaf area index (LAI), to further evaluate whether the performance of the optimized ORCHIDEE model is improved in terms of soil carbon and structural characteristics. *Yang et al*. [2007] produced a map of SOC density between 0 and 1 m in China according to the second national soil survey and regional field surveys [*National Soil Survey Office*, 1998]. Based on this map [*Yang et al*., 2007, Figure 3], we extracted the observed range of SOC at each of the forest sites. To make the model output comparable with the observations, we combined carbon in the litter and soil pools to compute the SOC density for both the prior and posterior simulations. Because the model does not simulate vertical profiles of SOC, we allocated all the simulated SOC density to the 0–1 m depth interval following *Todd-Brown et al*. [2013] who evaluated SOC stocks in the CMIP5 models. We used an independent data set of multiyear (2001–2013) mean aboveground forest biomass (AGB) in China obtained through integrating satellite products and ground measurements from a machine learning algorithm by *Yin et al*. [2015], to evaluate simulated AGB before and after the parameter optimization. Considering that the uncertainty of this data set is not provided, we also performed a comprehensive search on all available biomass data that are reported at each of the forest sites from the published papers (see Table S5). These studies are all conducted after the year of 2000, and the data can therefore represent the typical characteristics of AGB during the optimization year.

2.4.3. Simulation With Altered Temperature and Precipitation

To compare the difference in model responses to temperature (T) and precipitation (P) between prior and optimized simulations, we design a series of experiments driving the ORCHIDEE model with altered temperatures and precipitations in the meteorological forcing data set. For altered temperature scenarios, we define five sets of forcing: year-round temperature evenly (i.e., each value increased by a same magnitude through the whole time series) increased by 0 K (T, control simulation), 0.5 K (T + 0.5 K), 1 K (T + 1 K), and 2 K (T + 2 K). For altered precipitation, seven scenarios are considered where the relative precipitation amount is changed: year-round precipitation amount evenly decreases by 30% (P − 30%), 20% (P − 20%), 10% (P − 10%), and 0% (P, control simulation) and increases by 10% (P + 10%), 20% (P + 20%), and 30% (P + 30%). The simulations are performed using both the prior and posterior parameter set for each site during the year when the parameters are optimized but not during the other years. The optimization years were chosen because of a better performance of the model in reasonably simulating the seasonal cycle of forest carbon cycle at these sites.

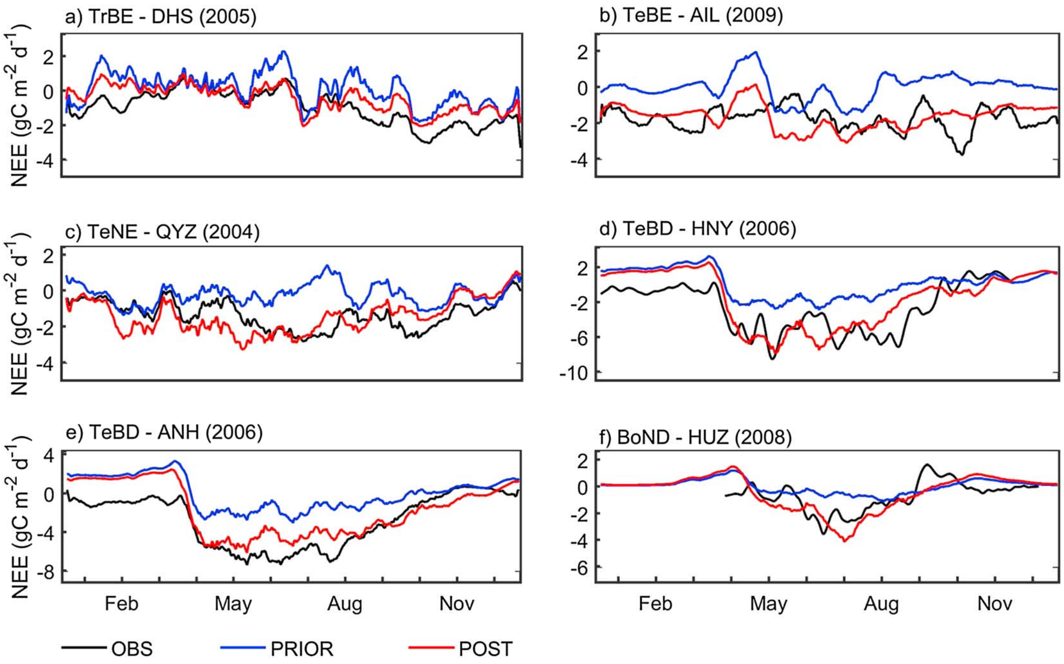

Figure 2. Seasonal cycle of the observations (OBS, black line), prior (PRIOR, blue line), and posterior (POST, red line) simulations of the net ecosystem exchange (NEE, gC m^{-2} d^{-1}) for each forest site for the optimization year. The curve is smoothed over a 15 day moving window.

Changes in the simulated net primary production (NPP), R_h, and NEE are illustrated in the results to show the impact of the optimized parameters on the transient response of the simulated carbon cycle to changed climate conditions.

Note that the hypothetical climate change scenarios are idealized since they do not consider the covariation among the climate variables. They are designed to be compared to the results from the forest manipulative experiments where only one environmental variable is often varied. The ecosystem response under realistic climate change projections [e.g., *T. Wang et al.*, 2014; *Wang et al.*, 2016] where covariation exists among climate variables is not accounted for currently but needs to be further explored. We also extracted the projected change (2081–2100 to 1986–2005) in MAT (K) and MAP (%) by climate models from the Coupled Model Intercomparison Projection phase 5 (CMIP5) under different Representative Concentration Pathways (RCPs) for each of the forest sites in China.

3. Results

3.1. Performance of the Optimized Model

3.1.1. Reduced Model Biases in NEE

For the prior simulation, NEE yearly mean is close to zero following the model spin-up (Figure 2). By contrast, observed NEE shows a net annual mean CO_2 uptake (i.e., negative NEE ranging from -1019.9 to -177.85 gC m^{-2} yr^{-1} across the sites). The prior simulations overestimate NEE for all PFTs, with a mean bias (i.e., MB) ranging from 0.41 to 3.09 gC m^{-2} d^{-1} (Table 1). The TrBE site has the lowest model-data mismatch with respect to NEE, with a MB and RMSE of 0.41 gC m^{-2} d^{-1} and 1.61 gC m^{-2} d^{-1}, respectively. By contrast, the largest biases in the prior NEE are found at the two TeBD sites, with MB and RMSE exceeding 3.0 gC m^{-2} d^{-1}. At the deciduous forest sites the simulated NEE seasonal amplitude is underestimated and the amplitude bias (AB) has a more negative bias at these sites (<-2.3 gC m^{-2} d^{-1}) than at the evergreen sites.

The optimized NEE shows a significant improvement in the model-data fit for all PFTs, with a mean RMSE reduction of 32% across the sites (Table 1). The TrBE, TeBE, TeNE, and TeBD sites all show a reduction in the RMSE of $>$30%, and the MB is reduced by 61% on average. The seasonal cycle of NEE is very well matched after optimization at the TrBE and TeNE sites (Figures 2a and 2c), indicating that optimized parameters can

Table 1. List of the Mean Biases (MB), Root-Mean-Square Error (RMSE), and Amplitude Biases (AB), Between the Simulated and Observed Daily Net Ecosystem Exchange (NEE, gC m^{-2} d^{-1}) for Each Plant Functional Type (PFT) Before (Prior) and After (Post) Parameter Optimization During the Optimization Year

	MB		RMSE		AB	
PFT	Prior	Post	Prior	Post	Prior	Post
TrBE	0.41	0.22	1.61	1.05	1.07	0.01
TeBE	1.76	0.12	2.39	1.56	0.03	−0.22
TeNE	1.41	−0.19	1.92	1.23	−0.81	0.48
TeBD(HNY)	3.09	1.08	3.78	2.47	−3.01	0.74
TeBD(ANH)	3.04	1.07	3.65	2.34	−2.44	0.23
BoND	0.66	−0.59	1.86	1.59	−2.37	0.34

explain the intra-annual variance of NEE for these two PFTs. Without considering the bias in mean value, the phase of the seasonal cycle of NEE is substantially improved after optimization at the TeNE, BoND, and two TeBD sites (Figure 3a). The modeled phase at TrBE site almost has no improvement after the optimization, indicating that the optimization reduces the prior biases only through reducing the annual mean NEE. The phase of the seasonal cycle at TeBE site is not well reproduced by both the prior and posterior simulations, probably because the meteorological forcing at this site is directly taken from the China forcing data set that might not well resolve the site-scale heterogeneity. Another cause for this mismatch between simulated and observed NEE may most likely be related to lack of quality control that leads to some unrealistic daily values in the observational records at this site. Ignoring that the NEE is overestimated during winter, a significant improvement of the seasonal cycle of NEE can also be found at the deciduous forest sites (Figures 2d–2f), in particular, for summer carbon uptake (see reduced AB in Table 1).

The reduced bias of NEE mainly reflects reduced values of parameter K_{SoilC} representing a reduction of the initial soil carbon pool (Figure 4a) and changes in parameters MR_c and GR_{frac} (Figures 4b and 4c) providing a reduction of autotrophic respiration (R_a) at the southern China subtropical forests (i.e., TrBE, TeBE, TeNE, and two TeBD sites). The reduced bias of NEE at the above sites (except for TrBE) and cool climate forests (i.e., BoND) also results from increased maximum photosynthetic rate parameters (i.e., Vcmax25, ARJV, and BRJV, i.e., intercept and slope of a linear function representing the ratio of Jmax25 to Vcmax25, Figures 4d–4f). More detailed discussions of parameter changes are given in section 4.1. The decreased respiration parameters have reduced (increased) the overall ecosystem respiration (R_{eco}) at sites in southern (northeast) China (Figure S1). We also use the observed diurnal amplitude of NEE to cross check the

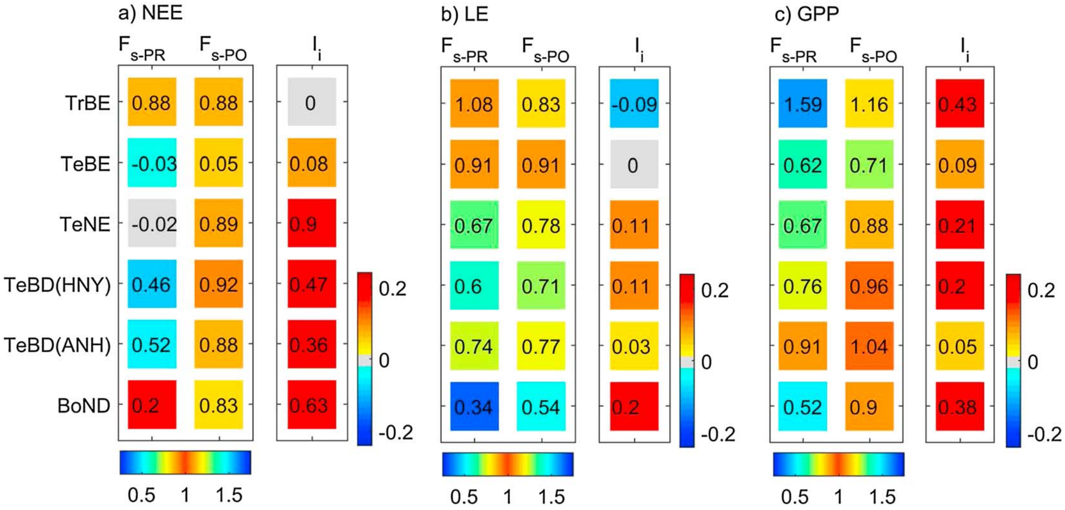

Figure 3. Agreement of the seasonal cycle (i.e., F_s) of the (a) net ecosystem exchange (NEE), (b) latent heat (LE), and (c) gross primary production (GPP) for the prior (PR), posterior (PO), and the I_i index indicating the improvement of the seasonal cycle at each forest site during the year when the model's parameters are optimized. For the best modal-data fit, the F_s should approach 1.

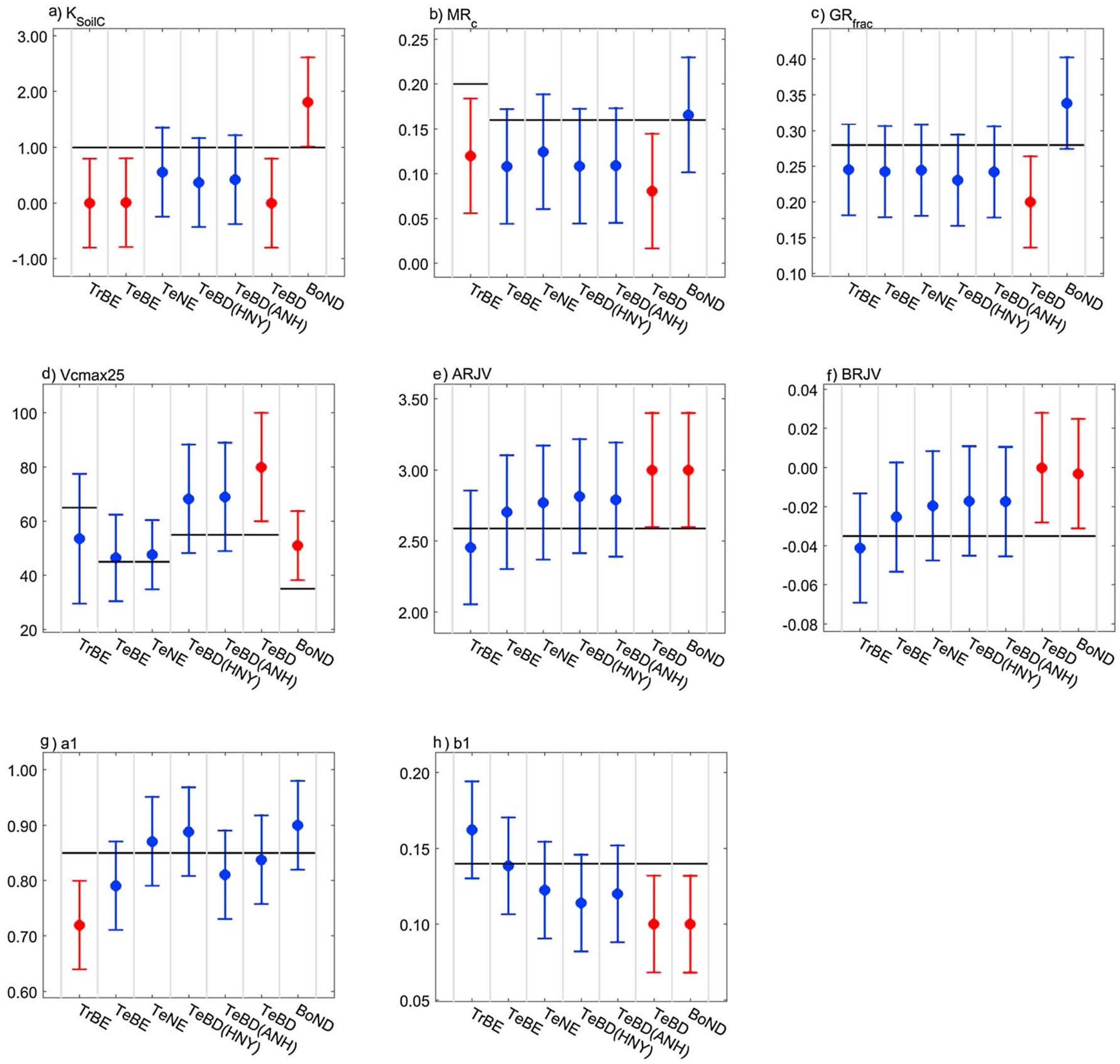

Figure 4. (a–h) Prior (black) and posterior (blue and red) values of some parameters related to soil respiration, autotrophic respiration, vegetation photosynthesis, and stomatal conductance (see Table S3) for the five plant functional types (PFTs). Note that the error bar for posterior values of each parameter denotes the posterior uncertainty produced by the data assimilation system and they are marked as red if the prior values are outside of this uncertainty. IDs shown on the *x* axis indicate the forest types corresponding to each of the forest sites listed in Table S1. Optimized parameter results for TeBD are obtained by assimilating both data from HNY and ANH sites.

optimized model that only assimilating daily eddy covariance data. With optimized parameters, daytime peak CO_2 uptake in the summertime (i.e., mean diurnal cycle) is enhanced at the QYZ TeNE, HUZ BoND, and two TeBD (HNY and ANH) sites, which improves the model fit to observed maximum daytime NEE (Figure S2).

3.1.2. Enhanced Performance of Simulated LE and GPP

Systematic model biases of LE and GPP are found at the TeNE, BoND, and the two TeBD sites, where the annual total LE is underestimated by 27%, 53%, and 25% (24%), respectively (Figures S3c–S3f and Table S6). This reflects the model shortcoming in capturing the summer high LE fluxes, possibly caused by plenty precipitation brought by the Asian monsoon. Summer GPP is also underestimated in the prior model run at these four sites (Figures S4c–S4f), reflecting the coupling between evapotranspiration (ET) and GPP from the model's equations. For two other sites, the model overestimates the GPP at the TrBE site (Table S7, MB for prior simulation: 5.12 gC m^{-2} d^{-1}), while it underestimates GPP at the BoND site (MB for prior simulation: -3.07 gC m^{-2} d^{-1}) according to the observations.

After the optimization, the underestimation of LE at the TeNE, BoND, and two TeBD sites in HNY (and in ANH) is reduced by 10%, 20%, and 8% (4%) of the observed LE, respectively. The enhanced performance of the simulated LE mainly occurs in summer, when GPP has also been improved at these four sites (Figures S4c–S4f). These results indicate that the optimization is more effective in improving simulations of the carbon and water fluxes, particularly in the productive season when temperatures are high. This is also supported by the improved diurnal cycle of the posterior simulations, with both peak daytime LE and GPP substantially enhanced at the QYZ TeNE, HUZ BoND, and two TeBD (HNY and ANH) sites and in better agreement with the observed amplitude of the summer mean diurnal cycle of these fluxes (Figure S2). In addition to increased maximum photosynthetic rates (Figures 4d–4f), the decreased value of parameter b1 (controlling the sensitivity of stomatal conductance to vapor pressure deficit, VPD) at the four sites (Figure 4h) enhances leaf-scale stomatal conductance at high VPD [*Yin and Struik*, 2009], which also matches the observed GPP (when GPP is included as a constraint, Figures S4c–S4f) and seasonal amplitude of NEE (Figures 2c–2f).

The phase of the seasonal cycle of LE and GPP from the prior simulations is in better agreement with observations than that of NEE (Table S8 and Figures S3 and S4). The correlation coefficients between the prior and observed LE and GPP are larger than 0.77 ($p < 0.001$) at all sites except for TeBE, indicating that the intra-annual variability of these fluxes is generally well captured by ORCHIDEE. On the other hand, the lower correlation ($R < 0.67$; daily values) of LE and GPP between prior simulations and observations at the TeBE site likely reflects the shortcoming of meteorological forcing which is directly taken from the China meteorological forcing data set. The model reasonably captures the seasonal cycle of LE and GPP at the TeBE site on monthly time scales (with generally low MB and RMSE, Tables S6 and S7), but the timing of daily variations is not properly captured at this site.

The optimized simulations further improve the model agreement for the seasonal cycle of LE and GPP. The agreement of the seasonal cycle (i.e., F_s) of the LE has been improved at four out of the six sites after the optimization, with the largest increase of F_s of 0.2 at the BoND site (Figure 3). The F_s of LE at the TeNE and two TeBD sites in HNY (and in ANH) has also been improved (i.e., shown by I_i) by 0.11 and 0.11 (0.03), respectively. On the other hand, the seasonal cycle of GPP is largely improved for all PFTs, with an improvement ranging from 0.05 to 0.43 (higher positive value denotes a greater improvement). Although the increased I_i of GPP has come at the expense of a decline in I_i of the LE at the TrBE site, its F_s of LE is still close to 1 (0.83 in Figure 3). The general enhancements of F_s (Figure 3) indicate a more reasonable seasonal cycle (e.g., the change from growing to nongrowing season) of simulated LE and GPP after the optimization at the forest sites in China (Figures S3 and S4).

Although the enhanced seasonal cycle performance is explained by improved fits to observed peak GPP and LE during summer time (Figures S3 and S4), the optimization of phenology-related parameters also adjusts the phase of these fluxes on the shoulder seasons. The directional changes of optimized phenology parameters are found qualitatively similar to other assimilation results using ORCHIDEE, with an increased specific leaf area (SLA, facilitating foliar development in the early season) and reduced LAI_{MAX} for the TeBD sites (Figures S5a and S5b) consistent with the result of a deciduous broadleaf forest in France [*Bacour et al.*, 2015]. Increasing the temperature threshold parameter that triggers earlier leaf senescence (Figure S5g) was also found by *MacBean et al.* [2015] in their normalized difference vegetation index-based optimization of phenology parameters. In contrast, the threshold of the growing degree days accumulation that sets leaf onset in deciduous forest is reduced for the site ANH having TeBD (Figures S5d–S5f), which is contrary to the increased threshold found by *MacBean et al.* [2015].

3.2. Validation of the Optimized Model

3.2.1. Cross-Year Validation

To examine the performance of the optimized model, we use the optimized parameters to simulate fluxes in other years. Figure 5 shows the RMSE of NEE, LE, and GPP over the years during which data are not used for optimization. Similar to the optimization year, the overestimated NEE predicted by the prior simulations in the other years is generally reduced (Figure S6), shown by a decreased RMSE between the observations and the model simulations (Figure 5) at most forest sites (except for the BoND where the sample size of high-quality observations in 2007 is quite small, Figure S6g). These results demonstrate the robustness of the optimized parameters in reducing the cross-year overestimation of the simulated NEE (RMSE is on average improved by 20%) in Chinese forest sites, with the largest improvement by 32% occurring at the TrBE site in 2004.

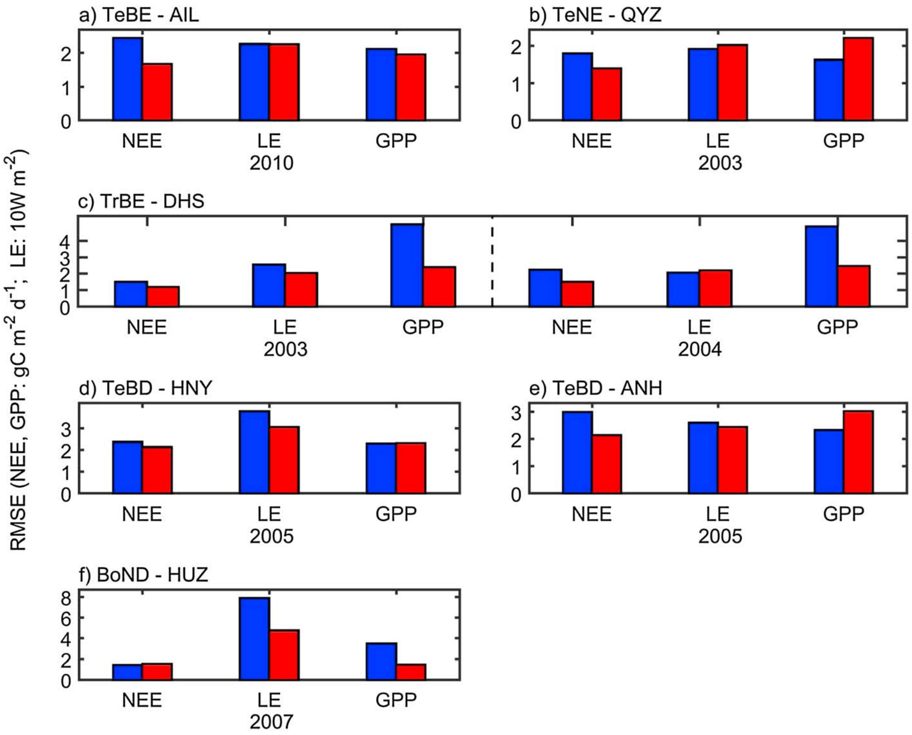

Figure 5. (a–f) Histograms of the root-mean-square error (RMSE) of the net ecosystem exchange (NEE, gC m^{-2} d^{-1}), gross primary production (GPP, gC m^{-2} d^{-1}), and latent heat (LE, 10 W m^{-2}) between simulations (prior, blue bar and posterior, red bar) and observations for each forest site during years when the model's parameters are not optimized.

The cross-year predictive ability of the optimized model in terms of the LE and GPP is likely dependent upon how large the reduction of RMSE is in the optimization year. For instance, the optimized parameters largely reduce RMSE of simulated LE by 31.33 W m^{-2} in the validation year (2007) at the BoND site (Figures 5f and S7g). This result is similar to the largely reduced RMSE of LE by 20.53 W m^{-2} in the optimization year (2008), and the optimized LE has a smaller RMSE compared to the observation errors at this site (i.e., 73.02 W m^{-2} in Table S6), implying that the optimized parameters have systematically improved the simulated LE at this site in different years. Another cross-year improvement of LE is found at the TeBD site in HNY (Figure S7e), where the optimized parameters in 2006 have reduced the RMSE by 7.22 W m^{-2} in the validation year of 2005. This reduction is even larger than the 5.75 W m^{-2} reduction in 2006 (Figure 5d and Table S6). For GPP, the cross-year predictive skill of the optimized parameters is found to be improved at the TrBE and BoND sites (Figures S8a, S8b, and S8g), where the RMSE is reduced by over 2 gC m^{-2} d^{-1} (Figures 5c and 5f), comparable to the reduced RMSE of over 2.15 gC m^{-2} d^{-1} at these two sites in the optimization year (Table S7). Overall, the RMSE is reduced on average by 11% for LE and by 14% for GPP among these forest sites, with the largest improvements by 40% and 58% at the BoND site in 2007 for LE and GPP, respectively.

3.2.2. Cross-Site Validation

Since the data from two TeBD sites are available, we investigate whether the error reduction by optimization of parameters at one site can be transferred to the other site for the same PFT as claimed by *Wang et al.* [2012]. Applying the parameters optimized by assimilating fluxes from ANH in 2006, the model predicts better NEE (and LE) at the HNY site for the same year, with RMSE reduced by 1.42 gC m^{-2} d^{-1} (and 1.53 W m^{-2}), which is within the observation errors (Table S9). Similar improvements are also found at the ANH site when the optimized parameters from the HNY site for 2006 are used, corresponding to a reduction in the RMSE of 1.37 gC m^{-2} d^{-1} and 8.04 W m^{-2} for NEE and LE, respectively. These cross-site validations suggest that the optimized model parameters which result in improvements in simulated NEE and LE can be transferred between the two TeBD sites, in particular, during the optimization year.

By contrast, the biases of the simulated GPP are only reduced for the site in HNY but not in ANH (Table S9). Since the optimization tends to increase simulated GPP at the site in ANH, we find that the GPP predicted by optimized parameters from HNY is overestimated at the end of the growing season (not shown).

To reduce the inconsistency between the two sites, we thus performed the multisite optimization by considering fluxes observed at the two sites in 2006 and obtained an optimized parameter set. Compared to directly applying the optimized parameters from the other site, applying parameters from the multisite optimization generally shows better performances at both of the two forest sites (Table S9). For the HNY site, the reduction in RMSE of NEE, LE, and GPP after the optimization can be as large as 42%, 13%, and 26%, respectively. Although the GPP bias is still large at the site in ANH (2.29 gC m^{-2} d^{-1}, 15% exceeding the observation errors), the multisite optimization has a lower RMSE compared to directly applying parameters from optimization at the site in HNY. The general improvements at the two TeBD sites suggest that the multisite optimization that contains information from both sites performs better in simulating the CO_2 and H_2O fluxes for simulation of TeBD.

3.3. Change in Responses of Carbon Cycling to Altered Temperature and Precipitation

To further test the impact of the optimization on responses of the ecosystem carbon cycling to climate change, we drive the model by incorporating parameters either before or after optimization under the designed scenarios of altered temperature and precipitation amount. Following previous studies [e.g., *Luo et al.*, 2008; *Peng et al.*, 2013b], we paid attention mainly on NPP, R_h, and NEE and to the effect of change in temperature and precipitation without accounting for their cross correlations, which vary upon climate regimes and may change between present day and future climate.

3.3.1. Change in Response to Warming

The response of the simulated NPP, R_h, and NEE to warming is almost linear at most forest sites (Figure 6), we thus define the mean sensitivity of NPP, R_h, and NEE to the increased temperature as a half of the difference of the annual values between the scenario of $T + 2$ K and the control simulation in the following paragraphs.

The annual NPP predicted by the prior simulations consistently declines with increased air temperature at sites from southern China, with a mean negative sensitivity of NPP to temperature ranging from −51.85 gC m^{-2} yr^{-1} K^{-1} to −10.69 gC m^{-2} yr^{-1} K^{-1} among these sites (Figures 6a, 6d, 6g, 6j, and 6m). This indicates that warming has an adverse impact on the simulated vegetation productivity of the southern forest ecosystem. On contrary, warming increases NPP simulated at the BoND site in northern China, where the prior NPP increases with the temperature at a rate of 10.63 gC m^{-2} yr^{-1} K^{-1}. Generally, this difference in the spatial pattern of the warming response remains after the parameter optimization, but the magnitude of the response is changed. The largest increase of the sensitivity of NPP to warming is found at the TrBE site (Figure 6a), where the temperature sensitivity of NPP has been increased (i.e., more negative) by 26.9 gC m^{-2} yr^{-1} in the optimized simulation. While the largest decline (i.e., less negative) of the temperature sensitivity of NPP occurs at the TeNE site (Figure 6g), where the sensitivity decreased by 15.36 gC m^{-2} yr^{-1} K^{-1} after the optimization. Relatively small changes of the magnitude of the temperature sensitivity of NPP are found at the two TeBD sites, with the temperature sensitivity of NPP increasing (i.e., more negative) by 6.27 gC m^{-2} yr^{-1} K^{-1} and reduced (i.e., less negative) by 13.54 gC m^{-2} yr^{-1} K^{-1} for the site in HNY and in ANH, respectively (Figures 6j and 6m).

The effect of optimization on annual NPP sensitivity to temperature depends on individual sensitivities of GPP and R_a. For example, an increase of parameters E_Vcmax and E_Jmax (Figures S5i and S5j) that makes maximum photosynthesis rates more responsive to a unit temperature increase in the modified Arrhenius formulation [see also *Medlyn et al.*, 2002] of ORCHIDEE, results in a larger positive sensitivity of GPP to temperature during the intra-annual cold time period and a larger negative sensitivity of GPP during the time when temperature is higher than the optimum temperature [*Medlyn et al.*, 2002]. As a result, the more negative temperature sensitivity of GPP at the TrBE site after optimization (Figure S9a) reflects the larger decrease in GPP during the warm time period within a year. In addition, the decreased value of parameter MR_c at the TrBE, TeBE, TeNE and two TeBD sites in southern China (Figure 4b) produces a consistent decrease in the positive temperature sensitivity of the maintenance respiration (R_m) [*Santaren et al.*, 2014, equation (A15)] (Figures S9b, S9e, S9h, S9k, and S9n) (see more detailed discussions in section 4.2).

The response of R_h to increased temperature is positive for the prior simulations and has a relatively small divergence when compared to NPP across different PFTs, with the mean sensitivity of respiration to warming ranging from 9.48 gC m^{-2} yr^{-1} K^{-1} to 14.87 gC m^{-2} yr^{-1} K^{-1} (Figures 6b, 6e, 6h, 6k, 6n,

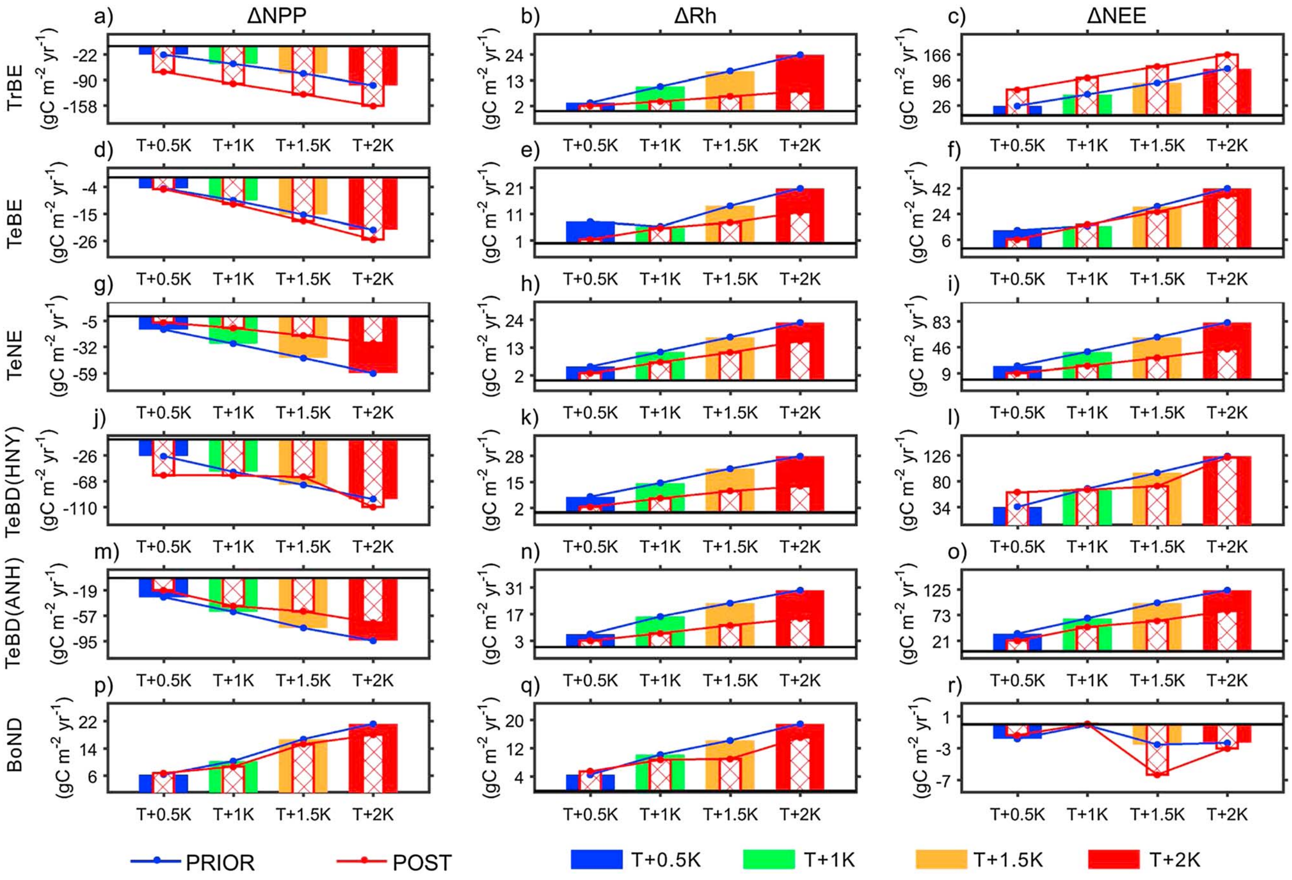

Figure 6. Modeled change in the (a, d, g, j, m, and p) net primary production (NPP, gC m^{-2} yr^{-1}), (b, e, h, k, n, and q) heterotrophic respiration (R_h, gC m^{-2} yr^{-1}), and (c, f, i, l, o, and r) net ecosystem exchange (NEE, gC m^{-2} yr^{-1}) under the four warming scenarios (T + 0.5 K, T + 1 K, T + 1.5 K, and T + 2 K) compared to the controlled simulations at the TrBE (Figures 6a–6c), TeBE (Figures 6d–6f), TeNE (Figures 6g–6i), TeBD (HNY) (Figures 6j–6l), TeBD (ANH) (Figures 6m–6o), and BoND (Figures 6p–6r) site (see ID and site names in Table S1). The prior simulation results are shown by the blue line (and colored bars), while the posterior simulation results are shown by the red line (and bars with red cross-hatching pattern).

and 6q). After the optimization, the positive sensitivity of R_h to warming is consistently reduced due to the decrease of parameter K_{SoilC} (Figure 4a) except for the HUZ site with BoND. In HUZ, the reduced temperature sensitivity of R_h is attributed to increased water stress after the optimization. The optimization causes a mean decrease of 44% in R_h sensitivity across all of the forest sites (Table S10). The maximum decrease of 7.76 gC m^{-2} yr^{-1} K^{-1} is found at the TrBE site and minimum decrease of 1.95 gC m^{-2} yr^{-1} K^{-1} occurs at the BoND site.

As a result of the balance between NPP and R_h, the simulated NEE generally increases with warming at forest sites in southern China for both the prior and posterior simulations (Figures 6c, 6f, 6i, 6l, and 6o), suggesting that the capacity of simulated carbon uptake at these sites is reduced with increased air temperature whether the parameters are optimized or not. Nonetheless, benefiting from consistently reduced R_h sensitivity, the response of NEE to warming is lessened after the optimization at the TeBE, TeNE, and two TeBD sites. For instance, the maximum decline in the response of NEE to warming is found at the TeBD site in ANH (Figure 6o), where the mean sensitivity of the annual NEE to warming declines by 20.99 gC m^{-2} yr^{-1} K^{-1}. While for another TeBD site in HNY, the mean sensitivity decrease by 1.24 gC m^{-2} yr^{-1} K^{-1} (Figure 6l). In contrast to NEE response to warming in southern China, the impact of parameters on simulated carbon cycling response is found much smaller for the BoND in northeast China (Figure 6r). This is because the response of NPP is comparable to that of R_h at this site; therefore, the direction of response of NEE to warming could be changed but the magnitude is quite small (Figure 6r). Overall, the mean sensitivity of NEE to warming decreases by 4.19 gC m^{-2} yr^{-1} K^{-1} after the optimization across all the forest sites in China.

3.3.2. Change in Response to Altered Precipitation Amount

To better quantify the water limitation on the carbon cycle, we also defined the sensitivity of fluxes to soil moisture variation as the slope of a linear regression between carbon flux and soil moisture anomalies, which are derived from the difference of annual values between six altered precipitation scenarios (i.e., $P - 30\%$, …, P + 30%) and the control simulation.

Except for two sites (i.e., the TrBE and BoND, Figures 7a and 7p) which are probably not water limited, the annual NPP in the prior simulations shows an asymmetric response with respect to the addition and removal of precipitation at four out of six forest sites (i.e., the TeBE, TeNE, and two TeBD sites, Figures 7d, 7g, 7j, and 7m). Large decreases of NPP are found for lower precipitation scenarios, while relatively small increases are found under increased precipitation (Figures 7d, 7g, 7j, and 7m). For instance, the decrease of annual NPP can be as large as -106.5 gC m^{-2} yr^{-1} under the scenario of $P - 30\%$ but the increase is only 13.69 gC m^{-2} yr^{-1} when increasing precipitation by 30% at the TeBE site. Similarly, the decline of the annual NPP simulated at the two TeBD sites exceeds 70 gC m^{-2} yr^{-1} under the lower precipitation scenario but its increase does not exceed 40 gC m^{-2} yr^{-1} even under the most abundant precipitation scenario. By contrast, the responses of the prior NPP show less sensitive to the altered precipitation amount at the TeNE site and are extremely small at the TrBE and BoND sites. The water stress at the TrBE and BoND sites is not severe, confirming that humid sites are less responsive to change in precipitation amount [*Gerten et al*., 2008]. The optimization does not change the asymmetric response at the four forest sites, although the magnitude of the response does change. The response of NPP to increase or decrease in precipitation amount is only slightly enhanced or diminished at the TeBE and TeNE sites (Figures 7d and 7g); by contrast, the response of NPP to altered precipitation amount is shown to be largely reduced (by 61%) at the ANH TeBD site but enhanced for the same PFT in HNY (Figures 7j and 7m). The different response at these two sites is due to decreased parameter $\mathrm{Hum}_{\mathrm{cste}}$, which alleviates soil moisture stress on photosynthetic rates and stomatal conductance at the ANH TeBD forest (Figure S5k), thus reducing the positive NPP sensitivity to soil moisture (Table S11). By contrast, this parameter is not optimized at the TeBD site in HNY and reduced soil moisture due to enhancement of LE (Figure S3d) increases the positive NPP sensitivity to soil moisture at this site (Table S11).

The impact of precipitation reduction on simulated R_h is consistent among all the forest sites, shown by the lower R_h predicted by the prior simulations ranging from -46.71 gC m^{-2} yr^{-1} to -13.55 gC m^{-2} yr^{-1} under the scenario of $P - 30\%$ (Figures 7b, 7e, 7h, 7k, 7n, and 7q). The optimization generally reduces this response at the TrBE (by 68%), TeBE (by 53%), TeNE (by 17%), BoND (by 59%), and the TeBD site in HNY (by 17%). In contrast, the negative impact (increase in R_h) of precipitation scenarios $P - 20\%$ and $P - 10\%$ is significantly enhanced at the TeNE site (Figure 7h).

By comparison, the increased precipitation scenarios generally result in a smaller increase in R_h than the precipitation depletion scenarios for the prior simulations. The optimization further reduces this smaller response for most PFTs except for the BoND where the response of R_h to increased precipitation is considerably enhanced by the optimized parameters (Figure 7q). Nonetheless, in southern China, again, the parameter optimization does not change the asymmetric responses of simulated R_h to altered precipitation amount but regulates the magnitude of the different responses at the various sites.

Because of the variable response of NPP and R_h to altered precipitation amount among the six forest sites, the response of NEE at these sites varies from site to site (Figures 7c, 7f, 7i, 7l, 7o, and 7r). These responses can be generally classified into three categories. First, the response of R_h to altered precipitation amount dominates that of NEE at the TrBE and BoND sites (Figures 7c and 7r), where the NPP shows almost no responses to the altered precipitation amount. The impact of the optimization on the responses of NEE is thus similar to those of R_h at the two sites. Second, the precipitation reduction has a larger impact on the NPP than on R_h at the TeBE and the two TeBD sites both for the prior and posterior simulations (Figures 7f, 7l, and 7o). The optimization at these three sites regulates the magnitude of the increased NEE (i.e., less carbon uptake) under the scenario of reduced precipitation amount and results in a lower NEE (more carbon uptake) under the abundant precipitation scenarios at the TeBE and TeBD in HNY. Third, the response of NEE to altered precipitation amount at the TeNE is dominated by that of R_h for the posterior simulations under the scenarios of $P - 20\%$ and $P - 10\%$, suggesting that the optimization tends to produce a more negative NEE under the conditions of less precipitation depletion at this site.

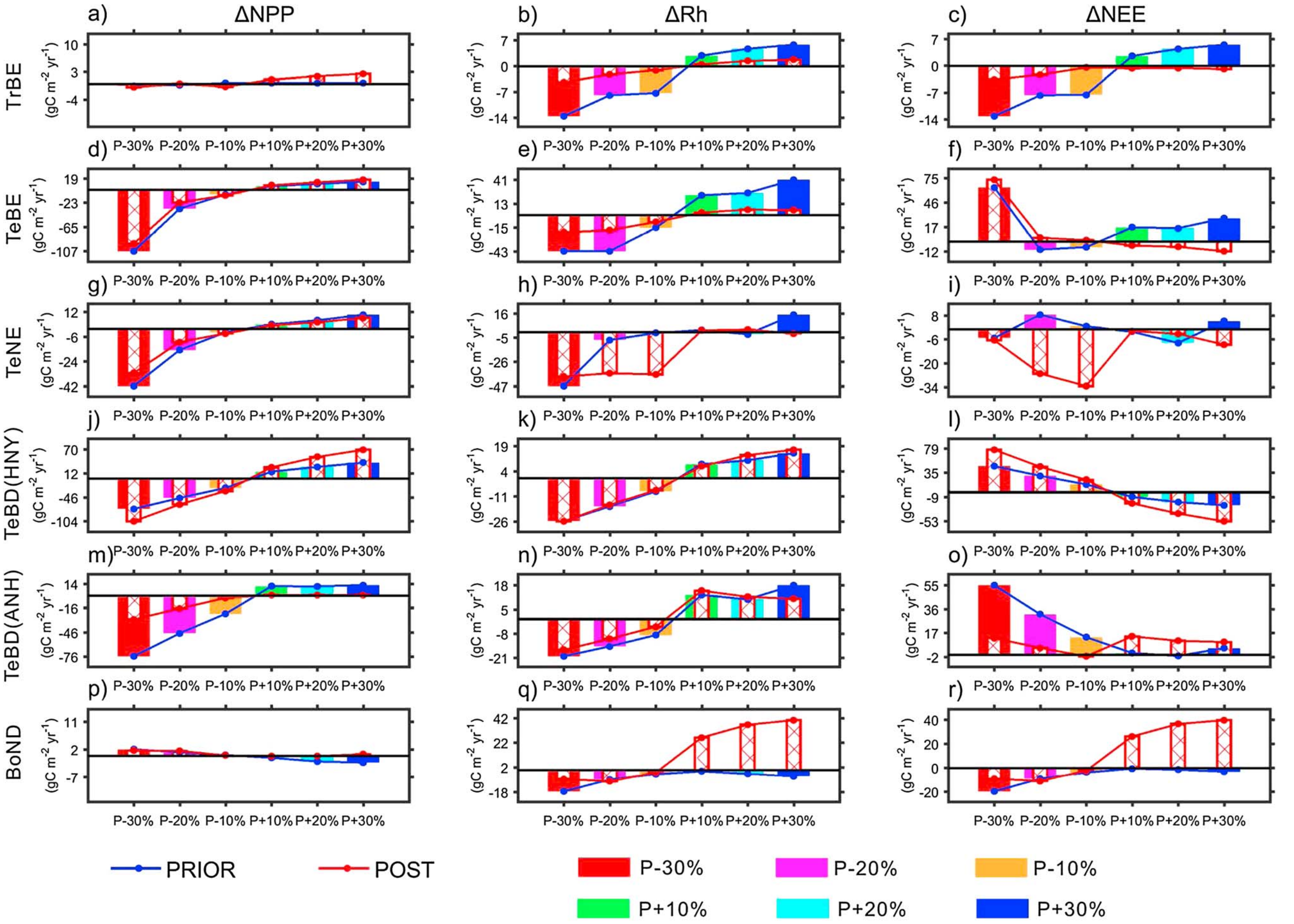

Figure 7. Modeled change in the (a, d, g, j, m, and p) net primary production (NPP, gC m^{-2} yr^{-1}), (b, e, h, k, n, and q) heterotrophic respiration (R_h, gC m^{-2} yr^{-1}), and (c, f, i, l, o, and r) net ecosystem exchange (NEE, gC m^{-2} yr^{-1}) under the six precipitation amount scenarios ($P - 30\%$, $P - 20\%$, $P - 10\%$, $P + 10\%$, $P + 20\%$, and $P + 30\%$) compared to the controlled simulations at the TrBE (Figures 7a–7c), TeBE (Figures 7d–7f), TeNE (Figures 7g–7i), TeBD (HNY) (Figures 7j–7l), TeBD (ANH) (Figures 7m–7o), and BoND (Figures 7p–7r) site (see ID and site names in Table S1). The prior simulation results are shown by the blue line (and colored bars), while the posterior simulation results are shown by the red line (and bars with red cross-hatching pattern).

4. Discussion

4.1. Impact of the Optimized Parameters on the Model Improvements

The results of this study show that the overestimated prior NEE simulations have been reduced (Figure 2), and the seasonal agreement of the LE and GPP is improved by the optimizations (Figure 3). These improvements are realized through optimizing parameters related to processes of the R_h, R_a, vegetation photosynthesis, and phenology (Table S3).

The observed NEE is not in equilibrium at a yearly time scale (Figure 2), which is opposite to the prior assumption of the model equilibrium state [*Pietsch and Hasenauer*, 2006; *Wutzler and Reichstein*, 2007; *Carvalhais et al.*, 2010; *Kuppel et al.*, 2014; *Peylin et al.*, 2016]. To reach a realistic nonsteady state initial condition, the optimization process reduces the value of parameter K_{SoilC} (Figure 4a) in order to diminish the size of the initial soil carbon pool and subsequently reduce simulated R_h, resulting in a net carbon sink. Decrease of this parameter is also reported by previous optimization studies mainly at TeBD and TeBE forest sites outside China [*Kuppel et al.*, 2012; *Bacour et al.*, 2015], showing that it is an effective parameter that accounts for past anthropogenic activity at each site that results in a nonequilibrium state (for example, forest management, logging, and land use change). Our results suggest that the optimization also reduces this parameter at the TrBE and TeNE sites (Figure 4a), reflecting the need to widely optimize this parameter at the southern forest sites in China.

Figure S10 shows the SOC density from prior and posterior model simulations and sampled from the inventory of SOC map from *Yang et al*. [2007]. Due to its SOC equilibrium assumption, the prior model gives a similar SOC density across the six forest sites ranging from 9.7 kg m^{-2} to 14.4 kg m^{-2}, overestimating SOC at the TrBE (in DHS), TeBE (in AIL), TeNE (in QYZ), and two TeBD (in HNY and ANH) sites in southern China and underestimating SOC at the BoND (in HUZ) site in northeastern China. The parameter optimization changes the K_{SoilC} (Figure 4a) that adjusts the seasonal amplitude and annual mean value of NEE, in a consistent direction to reduce biases of SOC density, with a reduction of RMSE reaching 39% across all forest sites (Figure S10). Yet at some sites like the DHS TrBE forest, optimized SOC becomes lower than the observation whereas the prior model simulation was consistent with the observation, probably suggesting a too fast turnover rate that is not optimized in this study. Given that the observed SOC density and its range shown in this study are still extrapolated based on a network of spatial SOC measurements, more accurate soil stock measurements near the forest sites are urgently needed to optimize parameters (e.g., residence time) related to the soil carbon pools.

On the other hand, the enhanced carbon uptake predicted by the optimized simulation can be partly attributed to decreased R_a during the growing season at the southern sites, as found in *Kuppel et al*. [2012] at 12 TeBD sites outside China, and evidenced by the reduction in MR_c and GR_{frac} values (corresponding to the reduced R_m and growth (R_g) respiration, respectively; Figures 4b and 4c). To further quantify the effect of the above respiration parameters (i.e., K_{SoilC}, MR_c, and GR_{frac}), we perform additional simulations during which the three respiration parameters are prescribed by prior values while the others are optimized. The results show that the RMSE of NEE is substantially increased at the TrBE site without considering effects of these respiration parameters. For the other forest sites in southern China, a large proportion of the reduced RMSE of NEE is found unable to be explained without considering effects of the respiration parameters (TeBE, 86%; TeNE, 21%; TeBD sites in HNY, 48%; and in ANH, 47%), suggesting the pervasive importance of these respiration parameter in southern China.

Although the optimized respiration parameters have been recognized as the most influential contributors to NEE in this study as well as a previous work on TeBD [*Kuppel et al*., 2012], we find that the optimization increases the maximum carboxylation capacity of Rubisco (V_{cmax}) and J_{max} (increasing with parameters called ARJV and BRJV in ORCHIDEE, Figures 4d–4f) are of comparable importance for the TeBD in this study. By using prior values of the three photosynthetic parameters (i.e., Vcmax25, ARJV, and BRJV) but optimized values of the others, we rerun the model at these two sites and find that 33% (35%) of the reduced RMSE of NEE in the optimized simulations in HNY (ANH) could be explained by the enhanced photosynthesis capacity. In fact, the effect of the optimized three photosynthetic parameters is quite clear across the other PFTs since we assimilated GPP data into the ORCHIDAS system, with the photosynthetic parameters increased at the TeBE, TeNE, BoND, and two TeBD sites, decreased at the TrBE site (Figures 4d–4f). Except for the TrBE site where the observed GPP is considerably smaller compared to other PFTs [*Liu et al*., 2015], other extratropical PFTs all tend to have higher net assimilation rate. Particularly for the BoND site, the photosynthesis capability is largely increased to make the simulation fit both the observed GPP and NEE at the BoND site (Figures 2f and S4f). The respiration parameters at this site thus have to be increased to enlarge the soil and vegetation respiration and offset the peak NEE uptake in summer.

Including GPP in the cost function might bias the optimized photosynthetic rate parameters (i.e., Vcmax25, ARJV, and BRJV) as the GPP is separated from observed NEE through standard partitioning method from *Reichstein et al*. [2005]. Although this is one of the most conventionally used methods that extrapolates nighttime R_{eco} into daytime and compute GPP through subtracting daytime R_{eco} by NEE, however, other flux-partitioning methods (e.g., fitting observed daytime NEE with light-response curve) [*Gilmanov et al*., 2003] indicate that the method-induced difference of estimated GPP could be as large as 47 gC m^{-2} yr^{-1} [*Lasslop et al*., 2010]. In particular, a recent isotope-based measurement in the Harvard forest has suggested that GPP could be overestimated by 25% during the first half (i.e., from June to July) of the growing season [*Wehr et al*., 2016]. To exclude any potential bias from the partitioned GPP, we thus performed additional parameter optimization using only observed NEE and LE data. We found that the model fit to daily NEE and LE after optimization are generally similar to that when including the partitioned GPP from NEE according to *Reichstein et al*. [2005] in the observational vector. Specifically, increased photosynthetic rate parameters are coherently found at the TeBE, TeNE, BoND, and two TeBD sites after optimization, with the parameter values, e.g., Vcmax25, differing by less than 16% between NEE-LE-based and NEE-LE-GPP-based optimization (Table S12). This result justifies our conclusion of the increased photosynthetic rate of the optimized model in Chinese temperate forests. In contrast, we observed the opposite change at the TrBE site for the photosynthetic parameters between the two optimization methods (Table S12 and Figures 4d–4f), suggesting that assimilating GPP would substantially influence the simulated photosynthesis capability in tropical forests, where the model skill should be further investigated in the future.

The enhanced photosynthetic capacity at the TeNE and TeBD sites is likely true because the stand ages of these sites are reported to be only 25 years (TeNE), 7 years (TeBD in HNY), and 18 years (TeBD in ANH) during the observation period [*Zhou et al*., 2011; *Yu et al*., 2014]. The young- to middle-aged forests in southern China generally have a high rate of carbon sequestration [*Pan et al*., 2004; *S. Wang et al*., 2011] and increased nitrogen deposition at this region may enlarge their carbon uptake capacity during the growing season [*Yu et al*., 2014]. By contrast, the photosynthetic parameters in old forests of the TrBE and TeBE sites are not increased as large as those at the young forest sites. On the other hand, plenty water resources brought by Asian monsoon further facilitate the carbon uptake capacity of the forests during the summertime, probably explained the enhanced photosynthesis at the extratropical young- and middle-aged forest sites. The young stand age and plenty summer precipitation thus explain the underestimated AB (Table 1), and summer photosynthesis (Figures S4c–S4f) predicted by the prior simulations at the TeNE, BoND, and two TeBD sites, especially contrary to previous findings that the RMSE at TeBD sites outside China is generally small [*Kuppel et al*., 2012]. Our results thus suggest that TEMs using prior or globally optimized parameters could underestimate the carbon sequestration capacity of the young- and middle-aged forests in China.

Besides, the increased total photosynthetic capacity might not be attributed to increased LAI after the optimization, since optimized LAI decreases at most other sites (DHS TrBE, −17%; AIL TeBE, 0%; HNY TeBD, −22%; ANH TeBD, −9%; and HUZ BoND, −5%; Figure S11), except for the QYZ TeNE site (+31%). We also used three independent satellite-derived LAI data (i.e., GLASS [*Liang and Xiao*, 2012], GLOBALMAP LAI [*Liu et al*., 2012], and AVHRR GIMMS3g [*Zhu et al*., 2013]) over forest sites to evaluate the optimized model in LAI simulations. But there is a large uncertainty in the magnitude and seasonal variations of LAI between different data sets (Figure S11); for example, at the AIL TeBE and ANH TeBD site, the model biases of annual mean LAI gauged by different products are in the range of 0.22–0.82 and 0.53–2.54, respectively. Despite of this large uncertainty, satellite-derived LAI can still tentatively suggest a limited capacity of ORCHIDEE to correctly simulate the LAI seasonal cycle (e.g., AIL TeBE, Figure S11b). This result highlights the necessity of improving simulation of canopy structure and carbon allocation to foliage, in particular, though consecutive in situ measurements of the LAI near the flux tower of Chinese forest sites in future studies.

We further evaluated the simulated AGB based on the observed biomass data from *Yin et al*. [2015] and published studies. There is a large uncertainty of AGB across the observation data sets and within the model-observation comparison (Figure S12). Reason for difference between observed data sets could be the choice of different plots, plot size, spatial heterogeneity of small-scale forests, and even the quality of remote sensing data [*Yin et al*., 2015]. Both prior and posterior models simulating an inconsistent AGB with observations would be anticipated since AGB is determined not only by photosynthesis but also by carbon allocation and mortality [*Friend et al*., 2014]. Unless we consider allocation-related parameters such as the tree residence time that needs to be constrained by consecutive biomass measurements [see also *Thum et al*., 2017] currently unavailable, the optimization-only assimilating eddy covariance flux data are not expected to improve the simulated AGB (Figure S12).

4.2. Impacts of the Optimized Parameters on Modeled Response to Warming

Climate warming affects ecosystem carbon uptake as a result of the balance between the annual R_h and NPP, whose response to increased temperature is negative over the middle to low latitudes but positive over the high latitudes [*Berthelot et al*., 2005; *Friedlingstein et al*., 2006; *Luo*, 2007; *Arora et al*., 2013]. The different spatial pattern of the response of NPP to warming (i.e., negative sensitivity in water limited regions and positive ones in temperature limited ones) and the R_h response in the optimization has been evidenced in Figure 6. The temperature sensitivity of NPP is negative for sites in southern China and positive for BoND in northeast China, where the NPP response to warming is more or less consistent to the large-scale observation evidence, shown by the positive correlation between satellite-derived vegetation index and the maximum temperature in wet and cool ecosystems [*Peng et al*., 2013a]. As the response of NPP to climate change depends on the balance between GPP and R_a ($R_m + R_g$) [*Piao et al.*, 2010], we first discuss the impact of optimized parameters on response of the annual GPP, R_m, and R_g to separate their contributions to NPP. And then the impact of the optimized parameters on the annual R_h is discussed.

Our results show that GPP in the prior simulations has a negative sensitivity to warming at four out of five forest sites in southern China (Figures S9a, S9g, S9j, and S9m), due to enhanced soil moisture stress and/or from the temperature exceeding the photosynthesis optimum value (see V_{cmax} and J_{max} in *Yin and Struik* [2009]). Note that these results only represent the hypothetical GPP sensitivity to warming but neglect the potential impact of changed precipitation. Therefore, we derive the projected change in temperature and precipitation for each of the forest sites under different RCPs from climate models of the CMIP5. In addition to warming, we found that most of CMIP5 climate models project a small increase of the MAP within about 10% (Table S13), which could reduce water stress and thereby weaken the negative GPP sensitivity to warming. By analyzing the intra-annual GPP response to warming, we found that the GPP increase with warming at the evergreen forest sites due to the enhanced photosynthetic enzymatic activity during winter and at deciduous forest sites due to their advanced date of leaf onset (in particular, for TeBD). However, these increases are all hidden by the adverse impact of warming during summertime except for two sites (TeBE and BoND) where the intra-annual maximum air temperature is relatively lower. The positive response of GPP to warming at these two sites (Figures S9d and S9p) clearly benefits from the enhanced photosynthetic enzymatic activity and extended growing season, respectively.

The impact of the optimized parameters on GPP response to warming is mainly attributed to variations in parameters related to limiting function of temperature (e.g., E_Vcmax and E_Jmax, the activation energy in the Arrhenius function). The change in E_Vcmax and E_Jmax after the optimization increases the sensitivity of V_{cmax} and J_{max} to temperature at the TrBE, TeBD (HNY), and BoND sites and decreases the temperature sensitivity at the TeBE site (Figures S5i and S5j, and S9a, S9j, and S9p). Although the E_Vcmax and E_Jmax are increased at the TeNE site, the increase of the positive GPP response to warming in winter offsets the increase of the negative temperature sensitivity during summertime. This leads to an unchanged annual GPP response to warming at the TeNE site. For the TeBD (ANH) site where E_Vcmax and E_Jmax are not selected but with three phenology parameters chosen from the Morris analysis (Figures S5d–S5f, and S5i and S5j), we find that the start date of the growing season has been advanced. The positive response of GPP to warming in spring offsets some of negative temperature sensitivity of GPP during summertime after the optimization, thus reducing the temperature sensitivity of the annual GPP at this site (Figure S9m).

In contrast to GPP, the impact of the parameters on responses of R_m to warming is much simpler. The reduced (increased) $\mathrm{MR_c}$ at sites in southern (northeast) China corresponds to reduced (increased) temperature sensitivity (Figures 4b and S9). For the R_g, the impact of the optimized $\mathrm{GR_{frac}}$ on R_g is clear shown at the TeNE, BoND, and two TeBD sites where reduced (increased) $\mathrm{GR_{frac}}$ corresponds reduced (increased) temperature sensitivity. For the TrBE and TeBE sites, the impact of optimized $\mathrm{GR_{frac}}$ may have been regulated by change in difference between assimilation inputs and maintenance respiration outputs to plant biomass after the optimization [*Santaren et al.*, 2014].

The consistent reduction in the sensitivity of R_h to warming (Figures 6b, 6e, 6h, 6k, 6n, and 6q) can be attributed to two factors. First, the reduced size of the soil carbon pool (i.e., reduced $\mathrm{K_{SoilC}}$, a fraction value determining the R_h) results in smaller increase of R_h under warmer scenarios, where larger R_h values are expected. Second, less soil moisture after the optimization is found, in particular, for the TeNE, BoND, and two TeBD sites, where the posterior LE has been shown to increase during summertime (Figures S3c–S3f). The R_h response to warming at these sites is thus lessened by the increased water limit, which is consistent with report of the in situ observations [*Yu et al.*, 2008]. With a plausible projected increase in precipitation within only 10% coincident to warming for most of forest sites (Table S13), the increased water limitation on R_h response to warming after optimization is likely to be more or less alleviated in particular at the TeNE, BoND, and two TeBD (HNY and ANH) sites. Although this phenomenon suggests that slightly increased precipitation in the future could adjust the magnitude of reduced R_h sensitivity to warming, however, conclusion of the reduced $\mathrm{K_{SoilC}}$ that results in smaller increase of R_h to warming at sites in southern China remains robust. By contrast, the large increase in R_h under the scenario of P + 10% at the BoND site (Figure 7q), due to the increased SOC after optimization, implies that 10% increase of MAP in future could reduce the water limitation and thereby increase R_h response to ideal warming scenario at the BoND site in northeast China.

As one of the mechanisms of future CO_2 released or uptake by the terrestrial ecosystem is determined by the kinetic sensitivity of photosynthesis and respiration to warming [*Luo*, 2007], impact of the optimized parameters on temperature sensitivity of the NPP and R_h influences the predicted response of the land carbon uptake to warming. Our results show that the impact of optimized parameter on temperature sensitivity of NPP is divergent among the sites due to complicated interactions of parameter impacts on GPP, R_m, and R_g as discussed above. By contrast, response of R_h to temperature is less divergent due to the model assumption that R_h increases with warming [*Luo*, 2007]. We further show that response of R_h to warming is consistently reduced by the optimization and the adverse impact of warming on carbon sink (i.e., negative NEE) is lessened at all extratropical forest sites (Figures 6f, 6i, 6l, 6o, and 6r), indicating that the optimized model in Chinese forest ecosystems would reduce predicted warming-induced carbon release in the future.

4.3. Impacts of the Optimized Parameters on Modeled Response to Altered Precipitation Amount

The model response of NPP to modified precipitation is asymmetrical at the water-limited forest sites (Figures 7d, 7g, 7j, and 7m). This asymmetric response as well as its dependence on humid/arid environment is qualitatively consistent with previous simulations at a grassland site [*Peng et al*., 2013b] and forest regions outside China [*Gerten et al*., 2008]. The reason can be that the response of soil moisture to altered precipitation amount is also asymmetric within TEMs because decreased precipitation causes the depletion in soil water, while increased precipitation may not always increase the soil moisture. Excessive precipitation will keep the soil water near saturation, and the surplus water will generate the surface runoff. This model mechanism thus indicates that the soil depletion/saturation is the main cause for the simulated asymmetric responses of forest ecosystem to altered precipitation amount.

The impact of optimized parameters on ecosystem response to altered precipitation could be achieved through either directly regulating the vegetation root profile or indirectly influencing the soil water availability. Direct influence of the reduction in parameter $\mathrm{Hum}_{\mathrm{cste}}$ (representing less water stress for vegetation root) can be evidenced by the TeNE and TeBD (in ANH) sites. Shown by reduced $\mathrm{Hum}_{\mathrm{cste}}$ after the optimization, NPP at the TeNE and TeBD (in ANH) sites are shown to be less vulnerable to the scenarios of reduced precipitation after the optimization (Figures 7g and 7m). On the other hand, the responses of NPP to reduced precipitation at the TeBE and TeBD (in HNY) are controlled by increased and reduced soil moisture condition, resulting from decreased and increased ET after the optimization (Figures S3b and S3d), respectively. Similarly, the significantly reduced R_h to altered precipitation amount is also found suffered from reduced soil moisture after optimization under scenarios of $P-20\%$ and $P-10\%$ at the TeNE site. The large increase in R_h under scenarios of increased P at the BoND site may reflect the effect of increased soil carbon pool once the water limitation is released after the optimization. These results thus indicate that the impact of optimized parameters on R_h response could be large under specific precipitation scenarios, emphasizing the importance of optimization for future simulations under changed precipitation scenarios.

5. Limitations and Future Directions

In this study, we show that the seasonal and diurnal cycles of NEE, LE, and GPP can be improved by assimilating short-term observations of daily eddy covariance fluxes at six forest sites in China. Comparison between independent observed and modeled SOC density suggests that the optimized soil carbon parameters improve SOC stock simulations. But these improvements are not similarly found in the divergent interannual performance of the optimized model, suggesting that assimilating 1 year eddy covariance flux data is insufficient to improve the simulations of interannual variability (also see untransferable model bias between different time scales in *Wang et al*. [2012], as also found by *Santaren et al*. [2014]. Thus, a limitation of this study is the current lack of available long-term eddy covariance data at forest sites in China.

Improving the ORCHIDEE structure still matters most for long-term carbon stock and its changes, in particular, nutrient- and age-related changes of photosynthetic rates, carbon allocation, and tree mortality (see recent development in *Bellassen et al*. [2010] and *Naudts et al*. [2015]). These “slow” processes are not accurately described in the current trunk version of ORCHIDEE. For instance, we found that photosynthesis maximum rates need to be substantially enhanced to match daily eddy covariance fluxes from young and middle-aged forest sites in China. But this enhancement cannot be achieved through parameter optimization because of the lack of model processes relating stand age and nutrient effects to photosynthetic rates. Future studies should focus on the evaluation [e.g., *Wang et al*., 2013] of the modified model (including new processes such as forest management and nutrient limitation) performance on simulating forest growth (e.g., stand biomass and LAI) once consecutive forest inventory data are available at Chinese forest sites.

How adjusting parameters to improve the seasonal cycle of fluxes alters the temperature/precipitation sensitivity of photosynthesis and respirations depends on the structure of the model, and the role of each parameter has been discussed in sections 4.1–4.3. The structure of ORCHIDEE is roughly similar to the one of other land-surface models (e.g., JSBACH, CLM, and JULES) that contributed to CMIP5 [*Ciais et al*., 2013] for photosynthesis and soil organic C decomposition, so that the identification of important parameters should be of general interest for other terrestrial models. Nevertheless, considering the response is quantified under simulations of the hypothetical evenly change in temperature and precipitation, the cross correlations between climate variables and seasonal distributions of change in temperature/precipitation make it hard to directly evaluate the results using observed measurements from the eddy covariance data. The evaluation thus calls for the manipulative ecosystem experiments in Chinese forests, with the other environmental variables unchanged when investigating the forest temperature/precipitation sensitivities. On the other hand, more complicated climate change scenarios with cross correlations between environmental variables could be used to further investigate the change of simulated flux sensitivity resulted from parameter uncertainty.

Acknowledgments
This study was supported by the National Natural Science Foundation of China (41530528 and 41561134016), the 111 Project (B14001), and National Youth Topnotch Talent Support Program in China. The authors would thank all the principal investigators of each forest site for sharing the flux and meteorological forcing data used in this study. We also thank Kun Yang for providing the China meteorological forcing data. The data from two sites in Hunan Yueyang and Anhui Huaining are downloaded from the global FLUXNET database (http://www.fluxdata.org/), data from the site in Qianyanzhou are downloaded from the AsiaFLUX (http://www.asiaflux.net/), and the data from the Dinghushan, are downloaded from the ChinaFLUX (http://www.chinaflux.org/enn/index.aspx). The station precipitation used for constraining the annual amount at each forest site is extracted from data set provided by the National Meteorological Information Center of China's meteorological administration (www.nmic.gov.cn). The high spatial resolution soil database is downloaded at the website of the Land-Atmosphere Interaction Research Group at Beijing Normal University (http://globalchange.bnu.edu.cn/research/soilw). We also appreciate the team from the ORCHIDEE Data Assimilation System (https://orchidas.lsce.ipsl.fr/index.php) for providing the code of the model and the model-data fusion framework. The optimization and simulations were performed on the platform of the national supercomputer center in Tianjin, China (http://www.nscc-tj.gov.cn/). We also acknowledge the climate modeling groups, the World Climate Research Programme's (WCRP) Working Group on Coupled Modeling (WGCM), and the Global Organization for Earth System Science Portals (GO-ESSP) (http://cmip-pcmdi.llnl.gov/cmip5/). Data of CMIP5 models were downloaded from ftp.ceda.ac.uk.

References

Antonarakis, A. S., J. W. Munger, and P. R. Moorcroft (2014), Imaging spectroscopy- and lidar-derived estimates of canopy composition and structure to improve predictions of forest carbon fluxes and ecosystem dynamics, *Geophys. Res. Lett.*, *41*, 2535–2542, doi:10.1002/2013GL058373.

Arora, V. K., et al. (2013), Carbon–concentration and carbon–climate feedbacks in CMIP5 Earth system models, *J. Clim.*, *26*(15), 5289–5314, doi:10.1175/JCLI-D-12-00494.1.

Bacour, C., et al. (2015), Joint assimilation of eddy covariance flux measurements and FAPAR products over temperate forests within a process-oriented biosphere model, *J. Geophys. Res. Biogeosci.*, *120*, 1839–1857, doi:10.1002/2015JG002966.

Baldocchi, D. (2008), TURNER REVIEW no. 15. "Breathing" of the terrestrial biosphere: Lessons learned from a global network of carbon dioxide flux measurement systems, *Aust. J. Bot.*, *56*(1), 1–26, doi:10.1071/BT07151.

Baldocchi, D., E. Falge, L. Gu, and R. Olson (2001), FLUXNET: A new tool to study the temporal and spatial variability of ecosystem-scale carbon dioxide, water vapor, and energy flux densities, *Bull. Am. Meteorol. Soc.*, *82*(11), 2415, doi:10.1175/1520-0477(2001)082<2415:FANTTS>2.3.CO;2.

Bellassen, V., G. Le Maire, J. F. Dhôte, P. Ciais, and N. Viovy (2010), Modelling forest management within a global vegetation model—Part 1: Model structure and general behavior, *Ecol. Model.*, *221*(20), 2458–2474, doi:10.1016/j.ecolmodel.2010.07.008.

Berthelot, M., P. Friedlingstein, P. Ciais, J. L. Dufresne, and P. Monfray (2005), How uncertainties in future climate change predictions translate into future terrestrial carbon fluxes, *Global Change Biol.*, *11*(6), 959–970, doi:10.1111/j.1365-2486.2005.00957.x.

Braswell, B. H., W. J. Sacks, E. Linder, and D. S. Schimel (2005), Estimating diurnal to annual ecosystem parameters by synthesis of a carbon flux model with eddy covariance net ecosystem exchange observations, *Global Change Biol.*, *11*(2), 335–355, doi:10.1111/j.1365-2486.2005.00897.x.

Byrd, R. H., P. Lu, J. Nocedal, and C. Zhu (1995), A limited memory algorithm for bound constrained optimization, *SIAM J. Sci. Comput.*, *16*(5), 1190–1208, doi:10.1137/0916069.

Carvalhais, N., M. Reichstein, P. Ciais, G. J. Collatz, M. D. Mahecha, L. Montagnani, D. Papale, S. Rambal, and J. Seixas (2010), Identification of vegetation and soil carbon pools out of equilibrium in a process model via eddy covariance and biometric constraints, *Global Change Biol.*, *16*(10), 2813–2829, doi:10.1111/j.1365-2486.2010.02173.x.

Chen, Y., K. Yang, J. He, J. Qin, J. Shi, J. Du, and Q. He (2011), Improving land surface temperature modeling for dry land of China, *J. Geophys. Res.*, *116*, D20104, doi:10.1029/2011JD015921.

Ciais, P., et al. (2013), Carbon and other biogeochemical cycles, in *Climate Change 2013: The Physical Sciences Basis. Contribution of Working Group I to the Fifth Assessment Report of the Intergovernmental Panel on Climate Change*, edited by T. F. Stocker et al., pp. 465–570, Cambridge Univ. Press, Cambridge, U. K., and New York.

Cramer, W., et al. (2001), Global response of terrestrial ecosystem structure and function to CO_2 and climate change: Results from six dynamic global vegetation models, *Global Change Biol.*, *7*(4), 357–373, doi:10.1046/j.1365-2486.2001.00383.x.

Friedlingstein, P., et al. (2006), Climate-carbon cycle feedback analysis: Results from the C4MIP model intercomparison, *J. Clim.*, *19*(14), 3337–3353, doi:10.1175/JCLI3800.1.

Friend, A. D., et al. (2007), FLUXNET and modelling the global carbon cycle, *Glob. Chang. Biol.*, *13*(3), 610–633, doi:10.1111/j.1365-2486.2006.01223.x.

Friend, A. D., et al. (2014), Carbon residence time dominates uncertainty in terrestrial vegetation responses to future climate and atmospheric CO_2, *Proc. Natl. Acad. Sci. U.S.A.*, *111*(9), 3280–3285, doi:10.1073/pnas.1222477110.

Gerten, D., et al. (2008), Modelled effects of precipitation on ecosystem carbon and water dynamics in different climatic zones, *Global Change Biol.*, *14*(10), 2365–2379, doi:10.1111/j.1365-2486.2008.01651.x.

Gilmanov, T. G., et al. (2003), Gross primary production and light response parameters of four Southern Plains ecosystems estimated using long-term CO_2-flux tower measurements, *Global Biogeochem. Cycles*, *17*(2), 1071, doi:10.1029/2002GB002023.

Groenendijk, M., et al. (2011), Assessing parameter variability in a photosynthesis model within and between plant functional types using global Fluxnet eddy covariance data, *Agric. For. Meteorol.*, *151*(1), 22–38, doi:10.1016/j.agrformet.2010.08.013.

He, J. (2010), Development of surface meteorological dataset of China with high temporal and spatial resolution, M.S. thesis, Inst. of Tibetan Plateau Res., Chin. Acad. of Sci., Beijing, China.

Huang, M., S. Piao, Y. Sun, P. Ciais, L. Cheng, J. Mao, B. Poulter, X. Shi, Z. Zeng, and Y. Wang (2015), Change in terrestrial ecosystem water-use efficiency over the last three decades, *Global Change Biol.*, *21*(6), 2366–2378, doi:10.1111/gcb.12873.

Jarvis, A. J., V. J. Stauch, K. Schulz, and P. C. Young (2004), The seasonal temperature dependency of photosynthesis and respiration in two deciduous forests, *Global Change Biol.*, *10*(6), 939–950, doi:10.1111/j.1365-2486.2004.00743.x.

Ju, W., S. Wang, G. Yu, Y. Zhou, and H. Wang (2010), Modeling the impact of drought on canopy carbon and water fluxes for a subtropical evergreen coniferous plantation in southern China through parameter optimization using an ensemble Kalman filter, *Biogeosciences*, *7*(3), 845–857, doi:10.5194/bg-7-845-2010.

Kaminski, T., R. Giering, and M. Heimann (1996), Sensitivity of the seasonal cycle of CO_2 at remote monitoring stations with respect to seasonal surface exchange fluxes determined with the adjoint of an atmospheric transport model, *Phys. Chem. Earth*, *21*(5), 457–462, doi:10.1016/S0079-1946(97)81142-1.

Knorr, W., and J. Kattge (2005), Inversion of terrestrial ecosystem model parameter values against eddy covariance measurements by Monte Carlo sampling, *Global Change Biol.*, *11*(8), 1333–1351, doi:10.1111/j.1365-2486.2005.00977.x.

Knorr, W., and M. Heimann (2001), Uncertainties in global terrestrial biosphere modeling: 1. A comprehensive sensitivity analysis with a new photosynthesis and energy balance scheme, *Global Biogeochem. Cycles*, *15*(1), 207–225, doi:10.1029/1998GB001059.

Krinner, G., N. Viovy, N. de Noblet-Ducoudré, J. Ogée, J. Polcher, P. Friedlingstein, P. Ciais, S. Sitch, and I. C. Prentice (2005), A dynamic global vegetation model for studies of the coupled atmosphere-biosphere system, *Global Biogeochem. Cycles*, *19*, GB1015, doi:10.1029/2003GB002199.

Kuppel, S., P. Peylin, F. Chevallier, C. Bacour, F. Maignan, and A. D. Richardson (2012), Constraining a global ecosystem model with multi-site eddy-covariance data, *Biogeosciences*, *9*(10), 3757–3776, doi:10.5194/bg-9-3757-2012.

Kuppel, S., P. Peylin, F. Maignan, F. Chevallier, G. Kiely, L. Montagnani, and A. Cescatti (2014), Model–data fusion across ecosystems: From multisite optimizations to global simulations, *Geosci. Model Dev.*, *7*(6), 2581–2597, doi:10.5194/gmd-7-2581-2014.

Lasslop, G., et al. (2010), Separation of net ecosystem exchange into assimilation and respiration using a light response curve approach: Critical issues and global evaluation, *Global Change Biol.*, *16*(1), 187–208, doi:10.1111/j.1365-2486.2009.02041.x.

LeBauer, D. S., D. Wang, K. T. Richter, C. C. Davidson, and M. C. Dietze (2013), Facilitating feedbacks between field measurements and ecosystem models, *Ecol. Monogr.*, *83*(2), 133–154, doi:10.1890/12-0137.1.

Le Quéré, C., et al. (2009), Trends in the sources and sinks of carbon dioxide, *Nat. Geosci.*, *2*(12), 831–836, doi:10.1038/NGEO689.

Liang S. and Z. Xiao (2012), Global land surface products: Leaf area index product data collection (1985-2010), Beijing Normal University, doi:10.6050/glass863.3004.db.

Liu, Y., R. Liu, and J. M. Chen (2012), Retrospective retrieval of long-term consistent global leaf area index (1981–2011) from combined AVHRR and MODIS data, *J. Geophys. Res.*, *117*, G04003, doi:10.1029/2012JG002084.

Liu, Z., Q. Shao, and J. Liu (2015), The performances of MODIS-GPP and-ET products in China and their sensitivity to input data (FPAR/LAI), *Remote Sens.*, *7*(1), 135–152, doi:10.3390/rs70100135.

Lu, M., et al. (2013b), Responses of ecosystem carbon cycle to experimental warming: A meta-analysis, *Ecology*, *94*(3), 726–738, doi:10.1890/12-0279.1.

Lu, X., Y. P. Wang, T. Ziehn, and Y. Dai (2013a), An efficient method for global parameter sensitivity analysis and its applications to the Australian community land surface model (CABLE), *Agric. For. Meteorol.*, *182*, 292–303, doi:10.1016/j.agrformet.2013.04.003.

Luo, Y. (2007), Terrestrial carbon-cycle feedback to climate warming, *Annu. Rev. Ecol. Evol. Syst.*, *38*, 683–712, doi:10.1146/annurev.ecolsys.38.091206.095808.

Luo, Y., et al. (2008), Modeled interactive effects of precipitation, temperature, and $[CO_2]$ on ecosystem carbon and water dynamics in different climatic zones, *Global Change Biol.*, *14*(9), 1986–1999, doi:10.1111/j.1365-2486.2008.01629.x.

MacBean, N., F. Maignan, P. Peylin, C. Bacour, F. M. Bréon, and P. Ciais (2015), Using satellite data to improve the leaf phenology of a global terrestrial biosphere model, *Biogeosciences*, *12*(23), 7185–7208, doi:10.5194/bg-12-7185-2015.

McGuire, A. D., et al. (2001), Carbon balance of the terrestrial biosphere in the twentieth century: Analyses of CO_2, climate and land use effects with four process-based ecosystem models, *Global Biogeochem. Cycles*, *15*(1), 183–206, doi:10.1029/2000GB001298.

Medlyn, B. E., et al. (2002), Temperature response of parameters of a biogeochemically based model of photosynthesis. II. A review of experimental data, *Plant Cell Environ.*, *25*, 1167–1179, doi:10.1046/j.1365-3040.2002.00891.x.

Medlyn, B. E., et al. (2015), Using ecosystem experiments to improve vegetation models, *Nat. Clim. Change*, *5*(6), 528–534, doi:10.1038/NCLIMATE2621.

Morales, P., T. Hickler, D. P. Rowell, B. Smith, and M. T. Sykes (2007), Changes in European ecosystem productivity and carbon balance driven by regional climate model output, *Global Change Biol.*, *13*(1), 108–122, doi:10.1111/j.1365-2486.2006.01289.x.

National Soil Survey Office (1998), *Soils of China* [in Chinese], China Agricultural Press, Beijing, China.

Naudts, K., et al. (2015), A vertically discretised canopy description for ORCHIDEE (SVN r2290) and the modifications to the energy, water and carbon fluxes, *Geosci. Model Dev.*, *8*, 2035–2065, doi:10.5194/gmd-8-2035-2015.

Pacala, S. W., G. C. Hurtt, D. Baker, P. Peylin, R. A. Houghton, R. A. Birdsey, L. Heath, E. T. Sundquist, R. F. Stallard, and P. Cias (2001), Consistent land-and atmosphere-based US carbon sink estimates, *Science*, *292*(5525), 2316–2320, doi:10.1126/science.1057320.

Pan, Y., T. Luo, R. Birdsey, J. Hom, and J. Melillo (2004), New estimates of carbon storage and sequestration in China's forests: Effects of age–class and method on inventory-based carbon estimation, *Clim. Change*, *67*(2–3), 211–236, doi:10.1007/s10584-004-2799-5.

Papale, D., et al. (2006), Towards a standardized processing of net ecosystem exchange measured with eddy covariance technique: Algorithms and uncertainty estimation, *Biogeosciences*, *3*(4), 571–583, doi:10.5194/bg-3-571-2006.

Pappas, C., S. Fatichi, S. Leuzinger, A. Wolf, and P. Burlando (2013), Sensitivity analysis of a process-based ecosystem model: Pinpointing parameterization and structural issues, *J. Geophys. Res. Biogeosci.*, *118*, 505–528, doi:10.1002/jgrg.20035.

Pappas, C., S. Fatichi, S. Rimkus, P. Burlando, and M. O. Huber (2015), The role of local-scale heterogeneities in terrestrial ecosystem modeling, *J. Geophys. Res. Biogeosci.*, *120*, 341–360, doi:10.1002/2014JG002735.

Peng, C., X. Zhou, S. Zhao, X. Wang, B. Zhu, S. Piao, and J. Fang (2009), Quantifying the response of forest carbon balance to future climate change in northeastern China: Model validation and prediction, *Global Planet. Change*, *66*(3), 179–194, doi:10.1016/j.gloplacha.2008.12.001.

Peng, S., et al. (2013a), Asymmetric effects of daytime and night-time warming on northern hemisphere vegetation, *Nature*, *501*(7465), 88–92, doi:10.1038/nature12434.

Peng, S., et al. (2013b), Precipitation amount, seasonality and frequency regulate carbon cycling of a semi-arid grassland ecosystem in Inner Mongolia, China: A modeling analysis, *Agric. For. Meteorol.*, *178*, 46–55, doi:10.1016/j.agrformet.2013.02.002.

Peng, S., et al. (2015), Benchmarking the seasonal cycle of CO_2 fluxes simulated by terrestrial ecosystem models, *Global Biogeochem. Cycles*, *29*, 46–64, doi:10.1002/2014GB004931.

Peylin, P., et al. (2013), Global atmospheric carbon budget: Results from an ensemble of atmospheric CO_2 inversions, *Biogeosciences*, *10*(10), 6699–6720, doi:10.5194/bg-10-6699-2013.

Peylin, P., et al. (2016), A new step wise carbon cycle data assimilation system using multiple data streams to constrain the simulated land surface carbon cycle, *Geosci. Model Dev.*, *9*(9), 3321–3346, doi:10.5194/gmd-9-3321-2016.

Piao, S., J. Fang, B. Zhu, and K. Tan (2005), Forest biomass carbon stocks in China over the past 2 decades: Estimation based on integrated inventory and satellite data, *J. Geophys. Res.*, *110*, G01006, doi:10.1029/2005JG000014.

Piao, S., J. Fang, P. Ciais, P. Peylin, Y. Huang, S. Sitch, and T. Wang (2009), The carbon balance of terrestrial ecosystems in China, *Nature*, *458*(7241), 1009–1013, doi:10.1038/nature07944.

Piao, S., et al. (2010), Forest annual carbon cost: A global-scale analysis of autotrophic respiration, *Ecology*, *91*(3), 652–661, doi:10.1890/08-2176.1.

Piao, S., et al. (2012), The carbon budget of terrestrial ecosystems in East Asia over the last two decades, *Biogeosciences*, *9*(9), 3571–3586, doi:10.5194/bg-9-3571-2012.

Piao, S., et al. (2013), Evaluation of terrestrial carbon cycle models for their response to climate variability and to CO_2 trends, *Global Change Biol.*, *19*(7), 2117–2132, doi:10.1111/gcb.12187.

Piao, S., et al. (2015), Detection and attribution of vegetation greening trend in China over the last 30 years, *Global Change Biol.*, *21*(4), 1601–1609, doi:10.1111/gcb.12795.

Pietsch, S. A., and H. Hasenauer (2006), Evaluating the self-initialization procedure for large-scale ecosystem models, *Global Change Biol.*, *12*(9), 1658–1669, doi:10.1111/j.1365-2486.2006.01211.x.

Potter, K. A., H. Arthur Woods, and S. Pincebourde (2013), Microclimatic challenges in global change biology, *Global Change Biol.*, *19*(10), 2932–2939, doi:10.1111/gcb.12257.

Prentice, I. C., X. Liang, B. E. Medlyn, and Y. P. Wang (2015), Reliable, robust and realistic: The three R's of next-generation land-surface modelling, *Atmos. Chem. Phys.*, *15*(10), 5987–6005, doi:10.5194/acp-15-5987-2015.

Raoult, N. M., T. E. Jupp, P. M. Cox, and C. M. Luke (2016), Land-surface parameter optimisation using data assimilation techniques: the adJULES system V1.0, *Geosci. Model Dev.*, *9*(8), 2833–2852, doi:10.5194/gmd-9-2833-2016.

Reichstein, M., J. Tenhunen, O. Roupsard, J.-M. Ourcival, S. Rambal, F. Miglietta, A. Peressotti, M. Pecchiari, G. Tirone, and R. Valentini (2003), Inverse modeling of seasonal drought effects on canopy CO_2/H_2O exchange in three Mediterranean ecosystems, *J. Geophys. Res.*, *108*(D23), 4726, doi:10.1029/2003JD003430.

Reichstein, M., et al. (2005), On the separation of net ecosystem exchange into assimilation and ecosystem respiration: Review and improved algorithm, *Global Changes Biol.*, *11*(9), 1424–1439, doi:10.1111/j.1365-2486.2005.001002.x.

Santaren, D., P. Peylin, N. Viovy, and P. Ciais (2007), Optimizing a process-based ecosystem model with eddy-covariance flux measurements: A pine forest in southern France, *Global Biogeochem. Cycles*, *21*, GB2013, doi:10.1029/2006GB002834.

Santaren, D., P. Peylin, C. Bacour, P. Ciais, and B. Longdoz (2014), Ecosystem model optimization using in situ flux observations: Benefit of Monte Carlo versus variational schemes and analyses of the year-to-year model performances, *Biogeosciences*, *11*(24), 7137–7158, doi:10.5194/bg-11-7137-2014.

Shangguan, W., Y. Dai, Q. Duan, B. Liu, and H. Yuan (2014), A global soil data set for Earth system modeling, *J. Adv. Model. Earth Syst.*, *6*, 249–263, doi:10.1002/2013MS000293.

Sheffield, J., G. Goteti, and E. F. Wood (2006), Development of a 50-year high-resolution global dataset of meteorological forcings for land surface modeling, *J. Clim.*, *19*(13), 3088–3111, doi:10.1175/JCLI3790.1.

Shugart, H. H., S. Saatchi, and F. G. Hall (2010), Importance of structure and its measurement in quantifying function of forest ecosystems, *J. Geophys. Res.*, *115*, G00E13, doi:10.1029/2009JG000993.

Sitch, S., et al. (2008), Evaluation of the terrestrial carbon cycle, future plant geography and climate-carbon cycle feedbacks using five dynamic global vegetation models (DGVMs), *Global Change Biol.*, *14*(9), 2015–2039, doi:10.1111/j.1365-2486.2008.01626.x.

Thum, T., et al. (2017), The potential benefit of using forest biomass data in addition to carbon and water flux measurements to constrain ecosystem model parameters: Case studies at two temperate forest sites, *Agric. For. Meteorol.*, *234*, 48–65, doi:10.1016/j.agrformet.2016.12.004.

Todd-Brown, K. E., J. T. Randerson, W. M. Post, F. M. Hoffman, C. Tarnocai, E. A. Schuur, and S. D. Allison (2013), Causes of variation in soil carbon simulations from CMIP5 Earth system models and comparison with observations, *Biogeosciences*, *10*(3), 1717–1736, doi:10.5194/bg-10-1717-2013.

Verbeeck, H., P. Peylin, C. Bacour, D. Bonal, K. Steppe, and P. Ciais (2011), Seasonal patterns of CO_2 fluxes in Amazon forests: Fusion of eddy covariance data and the ORCHIDEE model, *J. Geophys. Res.*, *116*, G02018, doi:10.1029/2010JG001544.

Wang, S., L. Zhou, J. Chen, W. Ju, X. Feng, and W. Wu (2011), Relationships between net primary productivity and stand age for several forest types and their influence on China's carbon balance, *J. Environ. Manage.*, *92*(6), 1651–1662, doi:10.1016/j.jenvman.2011.01.024.

Wang, T., et al. (2011), Controls on winter ecosystem respiration in temperate and boreal ecosystems, *Biogeosciences*, *8*(7), 2009–2025, doi:10.5194/bg-8-2009-2011.

Wang, T., et al. (2012), State-dependent errors in a land surface model across biomes inferred from eddy covariance observations on multiple timescales, *Ecol. Model.*, *246*, 11–25, doi:10.1016/j.ecolmodel.2012.07.017.

Wang, T., C. Ottlé, A. Boone, P. Ciais, E. Brun, S. Morin, G. Krinner, S. Piao, and S. Peng (2013), Evaluation of an improved intermediate complexity snow scheme in the ORCHIDEE land surface model, *J. Geophys. Res. Atmos.*, *118*, 6064–6079, doi:10.1002/jgrd.50395.

Wang, T., X. Lin, S. Peng, N. Cong, and S. Piao (2014), Multimodel projections and uncertainties of net ecosystem production in China over the twenty-first century, *Chin. Sci. Bull.*, *59*(34), 4681–4691, doi:10.1007/s11434-014-0613-y.

Wang, T., X. Lin, Y. Liu, S. Dantec-Nédélec, and C. Ottlé (2016), Causes of uncertainty in China's net primary production over the 21st century projected by the CMIP5 Earth system models, *Int. J. Climatol.*, *36*(5), 2323–2334, doi:10.1002/joc.4497.

Wang, X., et al. (2014), A two-fold increase of carbon cycle sensitivity to tropical temperature variations, *Nature*, *506*(7487), 212–215, doi:10.1038/nature12915.

Wang, X., T. Wang, D. Liu, H. Guo, H. Huang, and Y. Zhao (2017), Moisture-induced greening of the South Asia over the past three decades, *Glob. Chang. Biol.*, *00*, 1–11, doi:10.1111/gcb.13762.

Wang, Y., G. S. Zhou, B. R. Jia, S. Li, and S. H. Wang (2010), Comparisons of carbon flux and its controls between broad-leaved Korean pine forest and Dahurian larch forest in northeast China [in Chinese], *Acta Ecol. Sin.*, *30*(16), 4376–4388.

Wang, Y. P., D. Baldocchi, R. A. Y. Leuning, E. V. A. Falge, and T. Vesala (2007), Estimating parameters in a land-surface model by applying nonlinear inversion to eddy covariance flux measurements from eight Fluxnet sites, *Global Change Biol.*, *13*(3), 652–670, doi:10.1111/j.1365-2486.2006.01225.x.

Wang, Y. P., R. Leuning, H. A. Cleugh, and P. A. Coppin (2001), Parameter estimation in surface exchange models using nonlinear inversion: How many parameters can we estimate and which measurements are most useful?, *Global Change Biol.*, *7*(5), 495–510, doi:10.1046/j.1365-2486.2001.00434.x.

Wehr, R., et al. (2016), Seasonality of temperate forest photosynthesis and daytime respiration, *Nature*, *534*(7609), 680–683, doi:10.1038/nature17966.

Williams, M., et al. (2009), Improving land surface models with FLUXNET data, *Biogeosciences*, *6*(7), 1341–1359, doi:10.5194/bg-6-1341-2009.

Williams, M., P. A. Schwarz, B. E. Law, J. Irvine, and M. R. Kurpius (2005), An improved analysis of forest carbon dynamics using data assimilation, *Global Changes Biol.*, *11*(1), 89–105, doi:10.1111/j.1365-2486.2004.00891.x.

Wu, Z., P. Dijkstra, G. W. Koch, J. Peñuelas, and B. A. Hungate (2011), Responses of terrestrial ecosystems to temperature and precipitation change: A meta-analysis of experimental manipulation, *Global Change Biol.*, *17*(2), 927–942, doi:10.1111/j.1365-2486.2010.02302.x.

Wutzler, T., and M. Reichstein (2007), Soils apart from equilibrium-consequences for soil carbon balance modelling, *Biogeosciences*, *4*, 125–136, doi:10.5194/bg-4-125-2007.

Xiao, J., K. J. Davis, N. M. Urban, K. Keller, and N. Z. Saliendra (2011), Upscaling carbon fluxes from towers to the regional scale: Influence of parameter variability and land cover representation on regional flux estimates, *J. Geophys. Res.*, *116*, G00J06, doi:10.1029/2010JG001568.

Yang, Y., A. Mohammat, J. Feng, R. Zhou, and J. Fang (2007), Storage, patterns and environmental controls of soil organic carbon in China, *Biogeochemistry*, *84*(2), 131–141, doi:10.1007/s10533-007-9109-z.

Yin, X., and P. C. Struik (2009), C_3 and C_4 photosynthesis models: An overview from the perspective of crop modelling, *NJAS-Wagen. J. Life Sci.*, *57*(1), 27–38, doi:10.1016/j.njas.2009.07.001.

Yin, G., Y. Zhang, Y. Sun, T. Wang, Z. Zeng, and S. Piao (2015), MODIS based estimation of Forest aboveground biomass in China, *PLoS One*, *10*(6), e0130143, doi:10.1371/journal.pone.0130143.

Yu, G., et al. (2014), High carbon dioxide uptake by subtropical forest ecosystems in the east Asian monsoon region, *Proc. Natl. Acad. Sci. U.S.A.*, *111*(13), 4910–4915, doi:10.1073/pnas.1317065111.

Yu, G., et al. (2008), Environmental controls over carbon exchange of three forest ecosystems in eastern China, *Global Change Biol.*, *14*(11), 2555–2571, doi:10.1111/j.1365-2486.2008.01663.x.

Yu, G. R., X. F. Wen, X. M. Sun, B. D. Tanner, X. Lee, and J. Y. Chen (2006), Overview of China FLUX and evaluation of its eddy covariance measurement, *Agric. For. Meteorol.*, *137*(3), 125–137, doi:10.1016/j.agrformet.2006.02.011.

Zaehle, S., S. Sitch, B. Smith, and F. Hatterman (2005), Effects of parameter uncertainties on the modeling of terrestrial biosphere dynamics, *Global Biogeochem. Cycles*, *19*, GB3020, doi:10.1029/2004GB002395.

Zhang, P. C., Y. P. Zhang, Z. Zheng, Y. H. Liu, and Z. H. Tan (2010), Carbon storage and sequestration of tree layer in subtropical evergreen broadleaf forests in Ailao Mountain of Yunnan [in Chinese], *Chin. J. Ecol.*, *29*(6), 1047–1053.

Zhao, Y., et al. (2012), How errors on meteorological variables impact simulated ecosystem fluxes: A case study for six French sites, *Biogeosciences*, *9*(7), 2537, doi:10.5194/bg-9-2537-2012.

Zhou, J., et al. (2011), Carbon budget and its response to environmental factors in young and mature poplar plantations along the middle and lower reaches of the Yangtze River, China, *J. Food Agric. Environ.*, *9*(3&4), 818–825.

Zhu, Z., et al. (2013), Global data sets of vegetation leaf area index (LAI) 3g and fraction of photosynthetically active radiation (FPAR) 3g derived from global inventory modeling and mapping studies (GIMMS) normalized difference vegetation index (NDVI3g) for the period 1981 to 2011, *Remote Sens.*, *5*(2), 927–948, doi:10.3390/rs5020927.

Zhu, Z., et al. (2016), Greening of the Earth and its drivers, *Nat. Clim. Change*, *6*, 791–795, doi:10.1038/nclimate3004.